ARTI-21CR/605-50015-01
ORNL/TM-2005/277

EVALUATION AND MODELING OF SPLIT-SYSTEM AIR CONDITIONER PERFORMANCE UNDER EXTREME AMBIENT TEMPERATURES WITH R-410A OPERATING UP TO THE REFRIGERANT CRITICAL POINT

Final Report

December 2005

C. Keith Rice

OAK RIDGE NATIONAL LABORATORY
Residential Buildings and Equipment Research Program
PO Box 2008, Mail Stop 6070
Oak Ridge, Tennessee 37831–6070
Tel: 865-574-2016; Fax: 865-574-9338; E-mail: ckr@ornl.gov

Prepared for

AIR-CONDITIONING AND REFRIGERATION TECHNOLOGY INSTITUTE
4100 N. Fairfax Drive, Suite 200, Arlington, Virginia 22203

DISCLAIMER

This report was prepared as an account of work sponsored by the Air-Conditioning and Refrigeration Technology Institute (ARTI) under its "HVAC&R Research for the 21st Century" (21CR) program. Neither ARTI, the financial supporters of the 21CR program, or any agency thereof, nor any of their employees, contractors, subcontractors or employees thereof - makes any warranty, expressed or implied; assumes any legal liability or responsibility for the accuracy, completeness, any third party's use of, or the results of such use of any information, apparatus, product, or process disclosed in this report; or represents that its use would not infringe privately owned rights. Reference herein to any specific commercial product, process, or service by trade name, trademark, manufacturer, or otherwise, does not necessarily constitute nor imply its endorsement, recommendation, or favoring by ARTI, its sponsors, or any agency thereof or their contractors or subcontractors. The views and opinions of authors expressed herein do not necessarily state or reflect those of ARTI, the 21CR program sponsors, or any agency thereof.

Funding for the 21CR program provided by (listed in order of support magnitude):
- U.S. Department of Energy (DOE Cooperative Agreement No. DE-FC05-99OR22674)
- Air-Conditioning & Refrigeration Institute (ARI)
- Copper Development Association (CDA)
- New York State Energy Research and Development Authority (NYSERDA)
- Refrigeration Service Engineers Society (RSES)
- Heating, Refrigeration and Air Conditioning Institute of Canada (HRAI)

Available to the public from

U.S. Department of Commerce
National Technical Information Service
5285 Port Royal Road
Springfield, VA 22161
(703) 487-4650 or (800) 553-6847
E-mail: info@ntis.fedworld.gov
Web site: www.ntis.gov/support/ordernowabout.htm

Available to U.S. Department of Energy and its contractors in paper from

U.S. Department of Energy
Office of Scientific and Technical Information
P.O. Box 62
Oak Ridge, TN 37831
(423) 576-8401
E-mail: reports@adonis.osti.gov
Web site: www.osti.gov/contact.html

ORNL/TM-2005/277
ARTI-21CR/605-50015-01

EVALUATION AND MODELING OF SPLIT-SYSTEM AIR CONDITIONER PERFORMANCE UNDER EXTREME AMBIENT TEMPERATURES WITH R-410A OPERATING UP TO THE REFRIGERANT CRITICAL POINT

Final Report

December 2005

Author: C. Keith Rice

Prepared for

AIR-CONDITIONING AND REFRIGERATION TECHNOLOGY INSTITUTE
Under ARTI 21CR Program Contract Number 605-50015

CONTENTS

LIST OF FIGURES

LIST OF TABLES

ACKNOWLEDGEMENTS

This work was sponsored by the Air-Conditioning and Refrigeration Technology Institute under ARTI 21-CR Program Contract Number 605-50015 funded in part by DOE cooperative agreement DE-FC05-99OR22674. Supplemental funding was provided by the U.S. Department of Energy, Contract Number DE-AC05-00OR22725. We would like to note the support and feedback from those involved with the sponsoring organizations, including ARTI project managers Michael Blanford and Steven Szymurski, project monitoring members Mark Spatz, Barbara Minor, Lawrence Grzyll, ARTI subcommittee chair Dick Ernst, and DOE project manager Esher Kweller. Copeland Corporation was most helpful in providing additional compressor information through Stan Schumann, Jim Horn, and Ken Monier. Assistance provided by the system equipment manufacturer Lennox is also gratefully acknowledged. The author would like to thank Piotr Domanski, Mark McLinden, and Vance Payne, the NIST principal investigators on the parallel ARTI project tasks, for their many interactions and sharing of test data. The expert assistance of Erica Atkin in technical editing and report preparation is most appreciated.

Evaluation and Modeling of Split-System Air Conditioner Performance at Extreme Ambient Temperatures with R-410A Operating Up To the Critical Point

ABSTRACT

The air conditioning performance of R-410A, an HFC replacement for R-22, is reduced at higher-temperature ambient conditions relative to R-22. The primary purpose of this project was to improve and validate air conditioning equipment performance modeling using R-410A at elevated ambient temperatures up to the critical point. Our work complemented the equipment testing in a parallel ARTI project with equipment performance analysis, relevant modeling improvements, and with system performance comparisons to the Oak Ridge National Laboratory (ORNL) Heat Pump Design Model (HPDM). We found that the compressor performance of the tested systems at elevated ambient temperatures is degraded relative to the manufacturer's data under standard test conditions. Mainly because of this, an uncorrected model under-predicts R-410A performance drop-off at higher ambient temperatures. Comparing R-410A to R-22 at 125ºF ambient, we found 11% larger drop in energy efficiency rating (EER) and 5% in capacity, with a 6% larger increase in power. When these effects were accounted for in the model, there was good agreement in performance trends with ambient temperature. The ORNL HPDM, using calibration factors that varied linearly with ambient, was able to simulate the performance of the R-410A system up to within 1ºF of the critical temperature. Refrigerant subcooling was found to be maintained fairly constant with thermostatic expansion valve (TXV) control, dropping slowly at higher ambient temperatures.

The system performance at elevated ambient temperatures of variable vs. fixed opening refrigerant flow controls is also evaluated. TXV control has less drop-off in EER and capacity at higher ambient temperatures than with fixed-flow controls, especially compared to capillary tube control. This is primarily due to the smaller drop in subcooling with ambient. However, power draw with a TXV is higher than for fixed-flow controls because higher condenser pressures are maintained at elevated ambient temperatures.

Recommendations are made regarding research needed to better characterize the effects of reduced compressor shell cooling on compressor performance. Refrigerant line heat loss modeling was also identified as a need for better prediction of absolute performance at more extreme ambient temperatures. Improvements are also needed in capillary tube modeling for R-410A, as the ASHRAE generalized correlation for capillary tubes was found to have transport property related errors in its development.

INTRODUCTION AND SCOPE

R-410A is an HFC refrigerant selected by the HVAC industry to replace HCFC R-22, which is slated to be phased out in 2010 for new equipment and in 2020 for use in existing equipment. While R-410A has been demonstrated to provide equivalent to higher SEER values, initial analysis at higher ambient temperatures based on the refrigerant properties suggests that EER and capacity will drop off relative to R-22. This is in large part because R-410A has a lower critical temperature than R-22, at approximately 161ºF as compared to about 205ºF for R-22.

There is also the general concern as to how R-410A will perform as the condensing temperature approaches the critical point. Such is conceivable in rooftop applications in hot climates,

especially in cases where the condenser airflow may be restricted or where the condenser exit air may be inadvertently recirculated to the inlet in certain space-constrained locations.

Thus the need was identified by ARTI to investigate R-410A performance relative to R-22 and other potential operational issues as the critical temperature of R-410A was approached. Performance at higher ambient temperatures is also of increasing interest to utilities with regard to peak power draw requirements. There was also a related interest in comparing the measured performance to that predicted by public air conditioning models such as those developed by ORNL and the National Institute of Science and Technology (NIST).

The general purpose of our project was to improve and validate modeling of air conditioning equipment performance using R-410A at elevated ambient operation up to the critical point. Our part of the project complemented the equipment testing effort with equipment performance analysis, relevant modeling improvements, and with system performance comparisons to the ORNL HPDM.

During the course of our project, we worked closely with NIST to use test data they measured on R-22 and R-410A air conditioners in their larger, parallel ARTI project (Domanski and Payne) to test and model these systems at extreme ambient conditions. They tested two nominal 13-SEER, split system residential air conditioners using the same indoor and outdoor heat exchangers and TXV flow control. One used R-410A and the other R-22 and both used scroll compressors from the same manufacturer. We predicted at the project outset, with our minimally calibrated model, that the critical temperature would be reached with R-410A in this 13 SEER system at 145ºF ambient. This information was used by NIST to confirm the operating condition requirements for their environmental test chambers.

We provided an assessment of the data measured by NIST by looking closely at the refrigerant-side operating conditions, using them to study the heat exchanger, flow control, and compressor performance. Model improvements and appropriate calibrations to measured component performance to improve prediction of performance at high ambient temperatures were also part of the effort.

The simulation program that we used for our analysis was the Mark VI version of the DOE/ORNL HPDM. This program has been widely used by industry for HCFC refrigerants, but has had only limited validation with HFC R-410A, and none at ambient temperatures approaching its critical temperature. As the EER with R-410A theoretically falls faster with higher ambient temperatures than with R-22, it is important, especially to utilities, to have good predictions of EER, capacity, and especially power draw at these conditions.

MARK VI MODEL IMPROVEMENTS

Thermodynamic Property Improvements for R-410A

Improvements to the subcritical modeling of R-410A performance were made to the Mark VI development version of the DOE/ORNL HPDM. These included upgrades to the thermodynamic properties for R-410A. The latest extended Martin-Hou (M-H) equation-of-state (EOS) correlations from DuPont (1999), including subcooled refrigerant property equations, were fully implemented. The new subcooled enthalpy relations provide a significant improvement in cycle COP predictions over previous use of saturated enthalpies at the subcooled temperatures. The new relations also improved the saturated vapor and superheated vapor property calculations near the critical point.

The effect of the new pressure-dependent subcooled properties can be seen in Fig. 1 in the difference between the DuPont Enhanced M-H results (no pressure dependence) and the DuPont 2000 Extended M-H (with pressure dependence). Also in Fig. 1 is the under-prediction of cycle

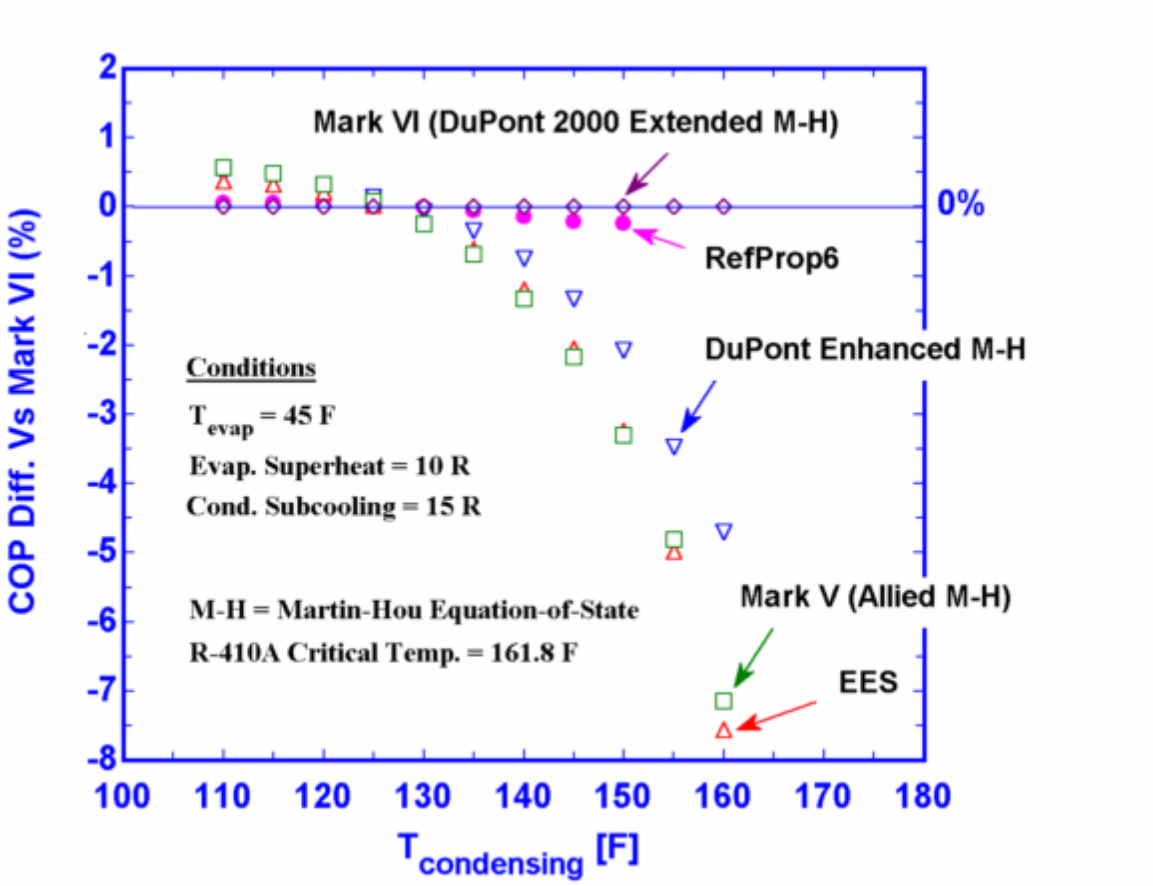

Fig. 1. Theoretical cycle COP comparisons for different R-410A representations up to near critical conditions.

COP at extreme ambient temperatures when using the previous distribution version of the ORNL model (Mark V) based on the last obtained Allied-Signal M-H coefficients (Rice and Jackson 1994); and those used by the Engineering Equation Solver (EES) program (Klein 1999). Variance between the Mark VI cycle COP values and those from RefProp 6.01 (McLinden et al., 1999) is seen to be less than 0.3% up to 150ºF, beyond which RefProp has difficulty converging on saturated properties. [Note that Allied-Signal (now Honeywell) currently uses RefProp-based properties.]

Using the new EOS correlations, theoretical predictions were made of R-410A vs. R-22 performance trends at higher condensing temperatures — normalized to 130ºF condensing for a 95ºF ambient typical of a low efficiency unit. These are shown in Fig. 2 for a fixed 45ºF evaporating temperature and fixed subcooling and superheat conditions. The capacity and EER drop-offs from R-410A exceed those for R-22 at higher temperatures by similar amounts while the power requirements are predicted to be nearly the same. For both refrigerants, EER is seen to

drop off the most as the capacity component of EER drops while power rises due to the higher pressure ratios.

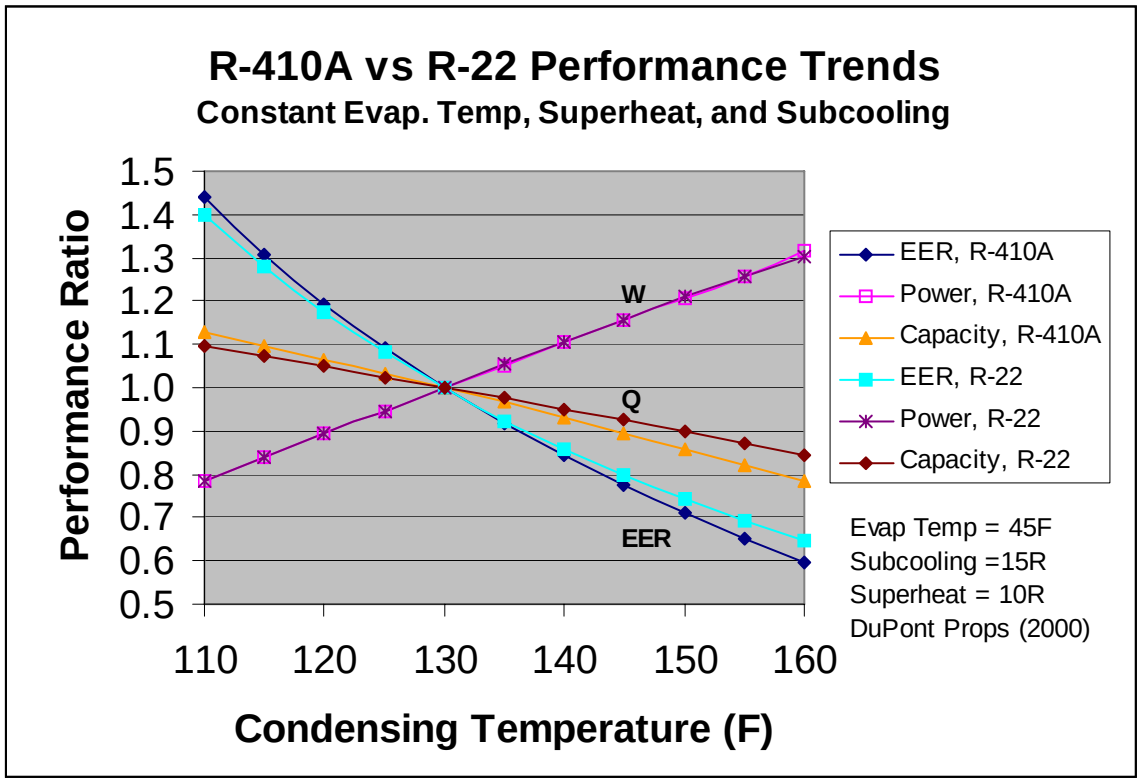

Fig. 2. Theoretical cycle performance trends for R-410A vs. R-22 for condensing temperatures up to 160ºF with fixed evaporating, superheating, and subcooling conditions.

Next the ORNL HPDM was exercised at ambient temperatures up to 135ºF for an R-410A window unit configuration previously tested at ORNL. The model was run under conditions of fixed refrigerant charge and flow controls (capillary tube and short-tube orifice), and trends were compared to test data for a fixed orifice control (needle valve) as shown in Fig. 3. This analysis demonstrated that the model could be run successfully to near critical condenser conditions and that the trends predicted for a short-tube orifice matched closely up to 115ºF with ORNL test data for a window unit. Predictions for a constant superheat/subcooling control (to approximate a TXV control) gave a higher condensing temperature and slightly higher power draw relative to the short-tube orifice case.

Improvements in Air Flow Rate Determination

We improved the way the model uses standard cfm (scfm) airflow data provided by manufacturers to calculate air mass flow rates and fan power with draw-through fans over a range of operating conditions. This involved determining within the program the volumetric airflow capability at the fan inlet (assumed to be a constant value derived from the rated scfm and reference fan inlet temperature). This fan characteristic is then used to determine the air mass flow at the current fan inlet operating conditions. Previously, the model determined air mass flow based on unit inlet rather than fan inlet airflows and conditions. In the revised approach, we specify the airflow as scfm based on a reference fan inlet temperature. This new approach results in a lower mass flow rate and fan power for typical outdoor draw-through units and thus should

give a more representative temperature rise prediction. The exit air temperature from the condenser is an important calculation in the determination of the saturation condensing temperature.

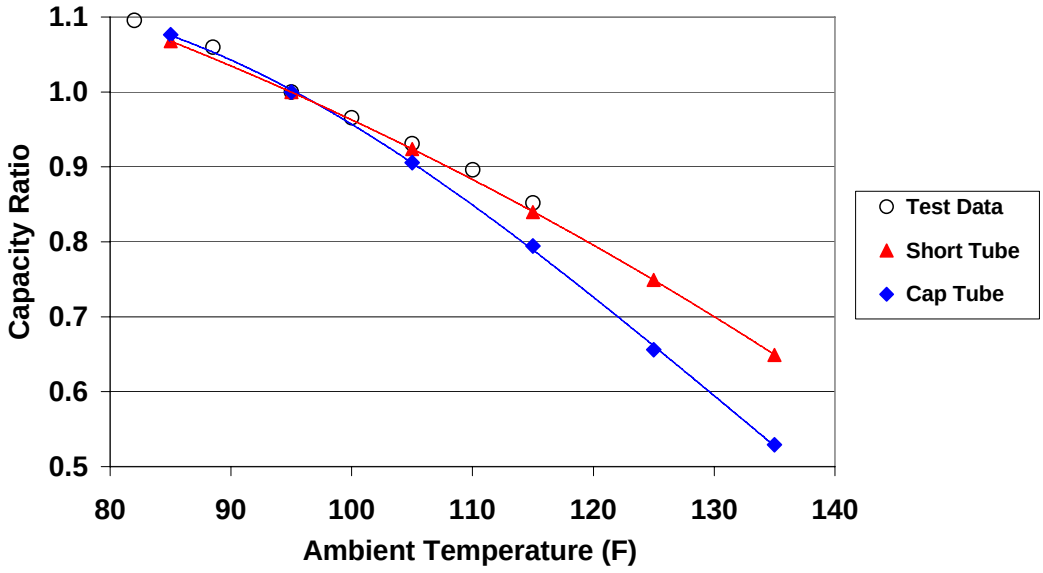

Fig. 3. Comparison of window A/C capacity ratios with R-410A predicted for short-tube orifice and capillary tube vs. test data with needle valve.

Refrigerant-Side Heat Transfer Correlation Improvements

The evaporating heat transfer correlations in the heat pump model were upgraded to use more HFC-suitable routines from Wattelet (1993) as modified and extended by Yokozeki and Bivens (1994). A similar upgrade to the HFC-tested condensing correlations was done with condensing heat transfer correlations from Dobson and Chato (1994). The choice of correlations for both evaporating and condensing (between the earlier Mark V and the newer correlations) was made an optional input selection, as was the point of vapor dryout in the evaporator. The choice of heat flux assumption for determining the average heat transfer coefficient over the range of refrigerant quality is also selectable internally to the code so that we can directly evaluate the effects of different assumptions. These ranged from constant heat flux to constant wall temperature to constant air-to-refrigerant temperature difference. The latter assumption was chosen to be most representative of typical one- to three-row cross-flow heat exchanger operation.

In testing the new correlations and heat flux assumptions we found that both had significant effects on the integrated average values. For R-410A, the new correlations of Dobson/Chato (1994) for condensing and Yokozeki/ Bivens for evaporating give 27% lower condensing and 35% lower evaporating coefficients than those in the previous Mark V version.

Improvement in Refrigerant Transport Properties at Saturation Temperatures Nearer the Critical Point

Overview

The refrigerant transport properties for four commercial HFC refrigerant mixtures including R-410A were upgraded to the most current available in a form suitable for inclusion in the ORNL Mark VI HPDM. These correlations are intended for use up to and beyond the critical point for R-410A and the other HFCs included (R-407C, R404A, R507C). We also upgraded the viscosity correlations for R-22.

The viscosity and thermal conductivity correlations for R-410A used in both the development (Mark VI) and the distribution (Mark V) versions of the ORNL HPDM were compared to RefProp6 and recently published correlations from Geller (2000). We also compared the R-22 viscosity correlations to those from RefProp6 and other sources. We found that the newer correlations gave significantly lower liquid viscosities for both refrigerants. The newer R-410A conductivity values are also higher than those used in Mark V.

From this comparison, we decided to upgrade Mark VI to use Geller's R-410A correlation. For the viscosity of R-22 liquid, we switched from an older ASHRAE (1976) correlation to a cubic representation to RefProp6 values. We also looked at the implication of the viscosity property differences on generalized correlations for capillary tubes and short-tube orifices and conclude that, at least for capillary tubes, an R-410A refrigerant-specific correlation will be significantly more accurate. The ASHRAE-recommended capillary tube model for use with R-410A is shown to under-predict flow rates when used with RefProp6 transport properties.

Comparison of R-410A Transport Property Correlations Up To the Critical Point — Viscosity

Semi-empirical engineering correlations recently developed by Geller (2000) for viscosity and thermal conductivity of R-410A (and other HFC mixtures) were evaluated for possible use in the ORNL model. These correlations are functions of temperature and density and represent properties over the subcooled, saturated, and superheated range. The viscosity correlations were shown by Geller to be within 2% over the tested range (up to 150°F) for liquid and vapor values while the conductivity values are within 4% (up to 140°F). The viscosity equations should be applicable to very near the critical point while the conductivity correlations will underestimate for reduced density values between 0.6 and 1.4 (within about 13°F of the critical region for liquid and within about 3°F for vapor).

We compared Geller's correlations for R-410A to:

- those used in the ORNL Mark V version (from Allied-Signal, 1993),
- those recently used in the ORNL Mark VI version, as given by DuPont in their engineering bulletins (ART-31, 1995 and 2000), and
- RefProp 6.01 (from NIST, 1999).

The viscosity comparisons are shown in Fig. 4 for saturated liquid and vapor properties of R-410A over a range of temperatures from evaporating to near critical (just above 160°F). Compared to the 1993 Allied predictions, all of the newer references give significantly lower liquid viscosities at all temperatures shown and predict higher vapor viscosities above 120°F. The percentage differences are shown in Fig. 5 and exceed 30% above 140°F. We find that the Geller correlation agrees closely with RefProp6 for viscosities up to the 153°F limit. Both the RefProp6

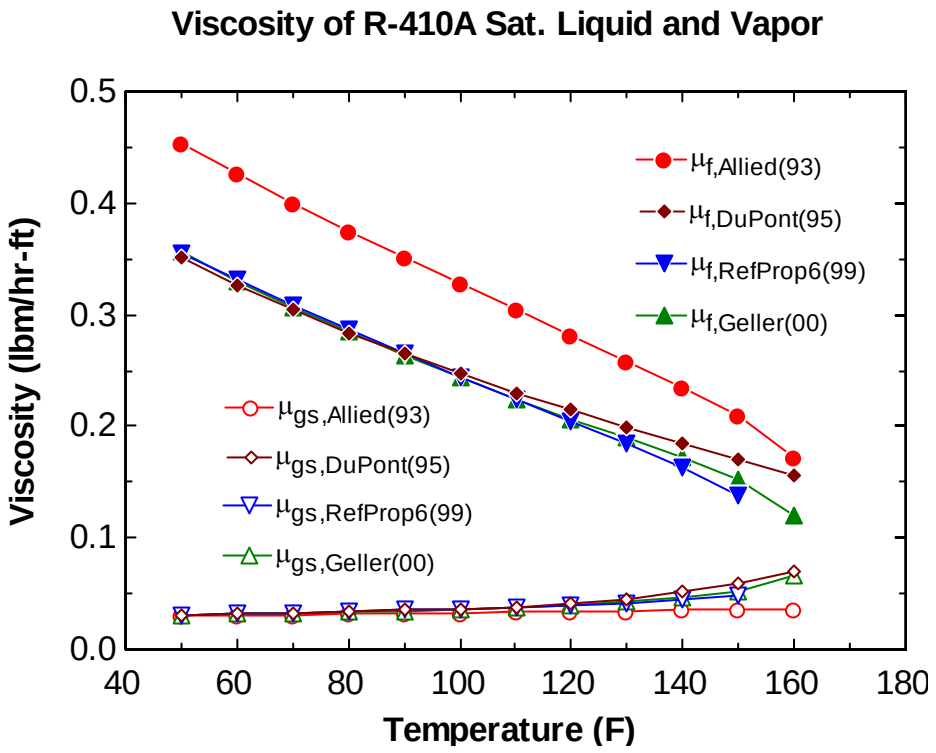

Fig. 4. Comparison of viscosity correlations for R-410A.

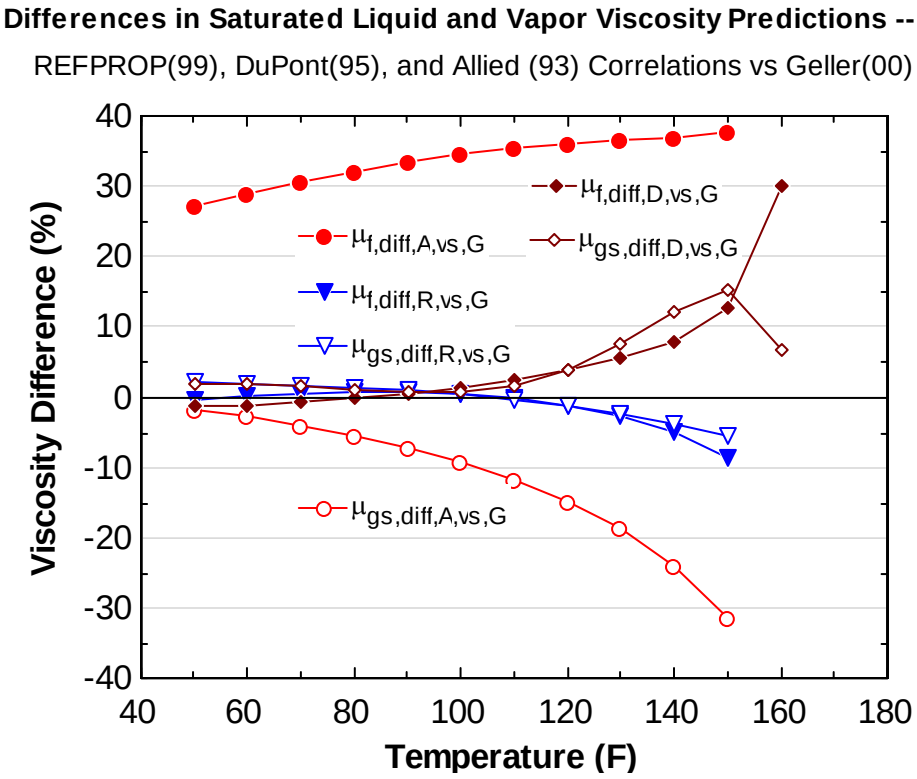

Fig. 5. Percentage differences between R-410A viscosity correlations.

and Geller correlations show trends of liquid and vapor values merging as the critical temperature is approached, while for the DuPont correlation the liquid viscosity approaches the Allied value above DuPont's quoted upper limit of 150°F. The Geller equation appears to be suitable for use on both sides of the critical region as long as the refrigerant density can be evaluated.

Effects of Viscosity Property Differences

It should be noted that the Allied viscosity correlations were commonly used in research projects in the mid-1990s where pressure drop and flow control correlations were developed. Two known examples of relevance to this project are the generalized correlation for capillary tubes developed by Wolf, Bittle, and Pate (1995, 1998) and that for short-tube orifice flow developed by Payne (1997).

Refrigerant Flow Control Correlations

The Wolf correlation is recommended for use with R-410A in the ASHRAE Refrigeration Handbook (1998). Figure 6 shows the effect of the viscosity difference on mass flow rate predictions from the Wolf correlation. Using RefProp6 viscosity values in the correlation gives an average mass flow under-prediction of about 11% compared to the original data. The generalized correlation for capillary tube flow most likely has a larger effect on viscosity differences than that for short-tube orifices does because the former uses liquid viscosity as a correlating parameter in most of the dimensionless groups. Also Payne (1997) developed a reduced-parameter form of his generalized equations, with slightly larger error bands, that does not appear to include viscosity as a parameter.

We presently use in the ORNL model a short-tube-orifice correlation specifically for R-410A, also developed by Payne (1999), which is not correlated to viscosity values and thus not subject to this issue. For capillary tube flow, we plan to use an R-410A specific correlation, also developed by Wolf (1995), that is tied to viscosity as a correlating parameter.

Comparison of R-410A Transport Property Correlations up to the Critical Point – Thermal Conductivity

Thermal conductivity comparisons are shown in Fig. 7 for saturated liquid and vapor properties of R-410A over the same range of temperatures. The agreement between the newer correlations is not nearly as close for conductivity as for viscosity where the RefProp6 values are generally higher, especially the vapor values. Geller's correlation shows stronger trends of liquid and vapor conductivity values merging as the critical temperature is approached. In contrast, in RefProp6, the vapor line rises sharply to approach the liquid line, which remains nearly linear.

Figure 8 shows the percentage differences in conductivity predictions with reference to the Geller correlation. The RefProp6 liquid values are 12 to 25% higher than Geller's, with the difference increasing with temperature. The RefProp6 vapor values are near those of Geller up to 90°F, increasing quickly up to 125% higher at 150°F. In contrast, the Allied vapor values are 40% lower at 150°F.

These changing values of thermal conductivity and viscosity since the early 1990's and the remaining uncertainty with current methods add to the error band in predictions of heat transfer and pressure drop correlations developed based on any specific property correlations.

Both of these newer references give significantly lower liquid viscosities, higher vapor conductivities, and generally higher liquid conductivities for R-410A than the earlier Allied

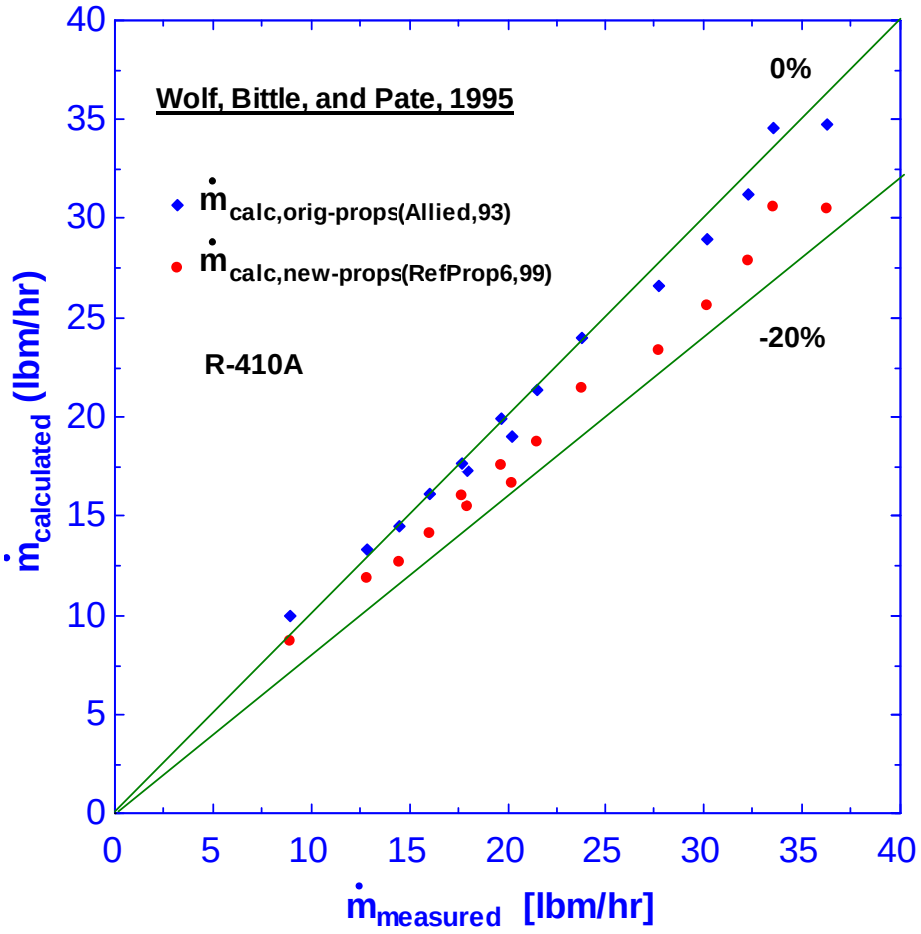

Fig. 6. Agreement between calculated and measured mass flow rates of R-410A through a capillary tube (case 2BRUN15) for Original Allied (93) and RefProp6 (99) viscosity values.

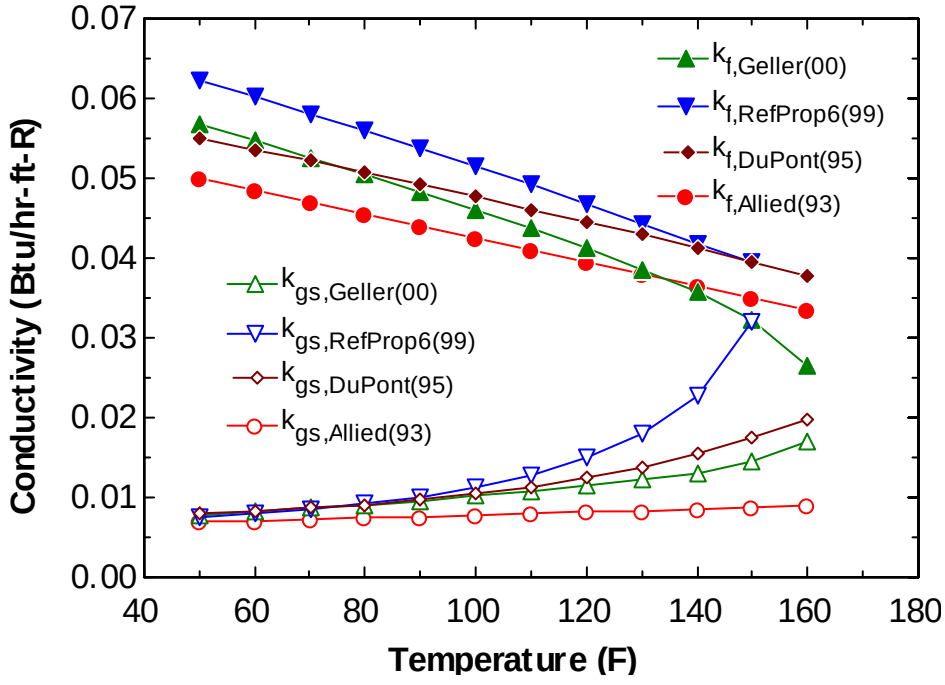

Fig. 7. Comparison of thermal conductivity correlations for R-410A.

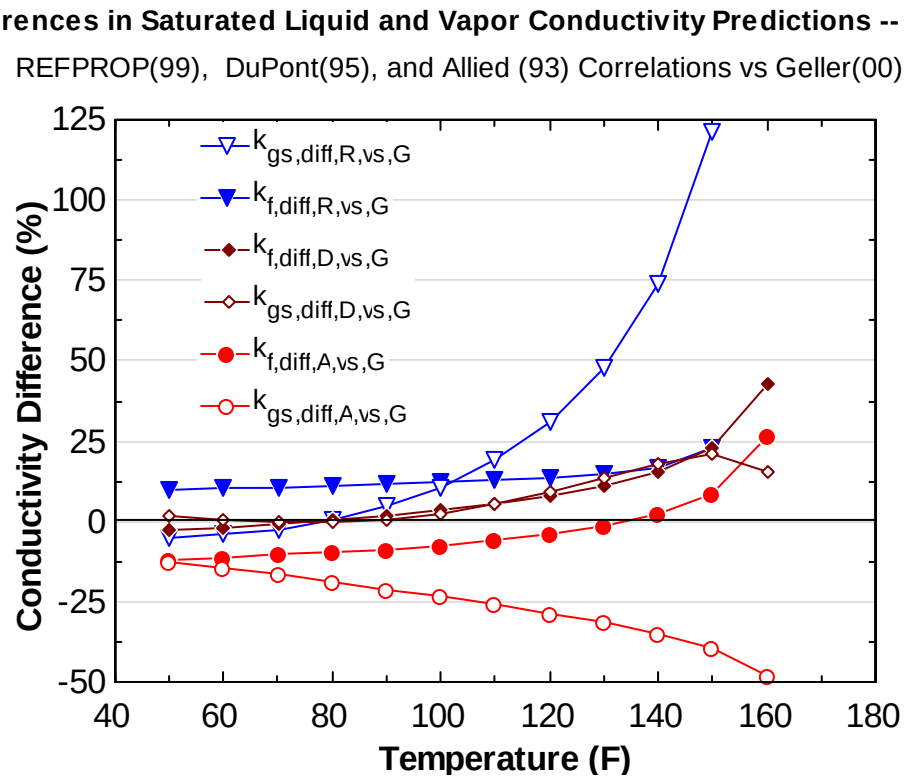

Fig. 8. Percentage differences between R-410A conductivity correlations.

predictions. As such, the cycle performance predictions for R-410A will be slightly higher because of these improved transport correlations.

Improvements in R-22 Transport Correlations

In the course of these property comparisons, we noticed that the liquid viscosities predicted by RefProp6 for R-22 were also somewhat lower that those used for some time in our model. On further checking, we found that there had been significant change in these values since publishing of the second edition of ASHRAE's *Thermophysical Properties of Refrigerants* (1976). Comparisons were made to the third edition of the ASHRAE publication (1993), which contains a liquid correlation recommended only for a more restrictive temperature range of –20 to 40°C (–4 to 104°F), than the values used in EES (Klein 1999) and RefProp6 (1999). Comparisons were also made to saturated vapor values, where the ASHRAE 1993 correlation was recommended only from –20 to 20°C (–4 to 68°F).

The comparisons are shown in Fig. 9 for a temperature range from –60°F to the critical temperature of 205°F. It is seen that while the vapor values show rather close agreement below160°F, the liquid values are significantly over-estimated above 60°F by the ASHRAE (1976) and EES correlations. (The EES liquid correlation has an upper limit of 152°F). (We should note that newer versions of Klein (2000) have a high accuracy property option for R-22 based on the correlations of Assael (1999), which we understand matches RefProp6 values quite closely as well.) The ASHRAE 1993 viscosity correlation for liquid matches with RefProp6 quite well between –20 and 150°F.

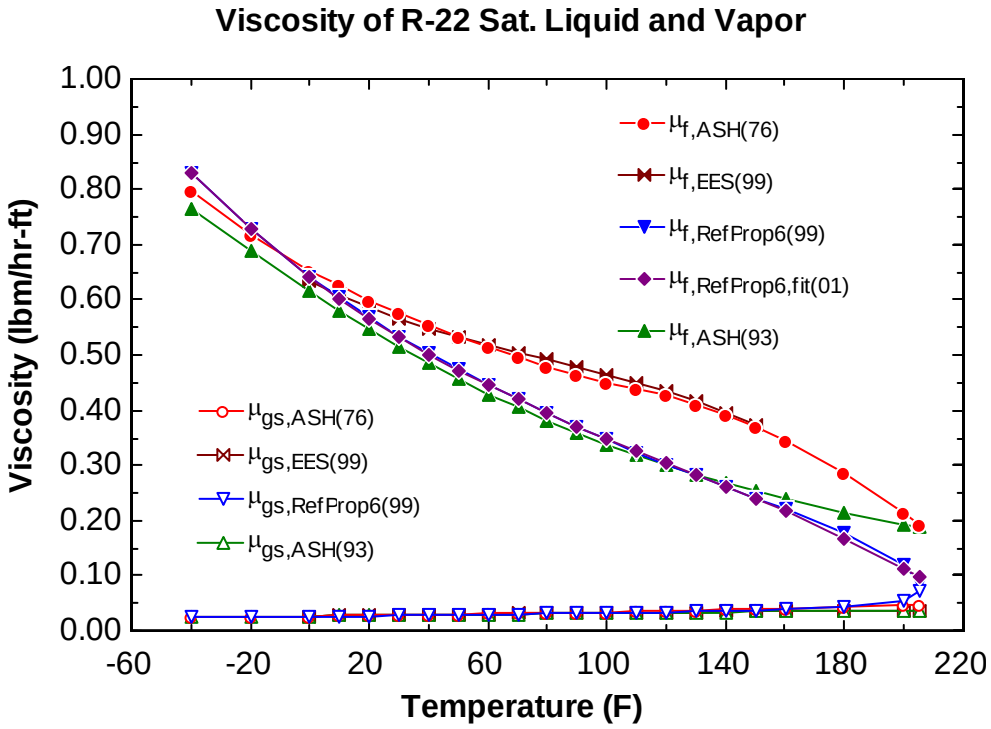

Fig. 9. Comparison of viscosity correlations for R-22.

As neither correlation was sufficiently close to RefProp6 over a broader temperature range, we fit a cubic polynomial in temperature to RefProp6 values from –40°F to 205°F for use in our Mark VI model for R-22 liquid viscosity. This curve fit is shown in Fig. 9 to match the RefProp6 values quite closely, with an RMS error of 4.18E-03. For the vapor values, we will stay with the ASHRAE (1976) correlation for now. In Fig. 10, the percentage differences between the various viscosity correlations for R-22 are shown. Here the saturated liquid properties from the new approach are seen to have significant improvement above 80°F.

For R-22 thermal conductivity values, the agreement between references is much closer for saturated properties and so we made no changes here.

Summary of Transport Property Changes

The new viscosity and conductivity correlations of Geller (2000) for HFC mixtures and the new liquid viscosity curve fit for R-22 were implemented in the Mark VI program. We understand that Klein (2000) also used the Geller correlations for the four HFC mixtures. [Note: Since this work was done, the Geller (2000) correlations have been further updated in a later ASHRAE 1142-TRP project by Geller (2002). These have not yet been included in the Mark VI HPDM.]

Since the new R-22 liquid viscosity values also give significantly lower liquid viscosities than the ASHRAE (1976) predictions, the net change in relative performance predictions between R-410A and R-22 will be reduced and based mainly on the higher R-410A conductivity values. The effects of new viscosity properties on the flow predictions through capillary tubes using the ASHRAE-recommended correlation are estimated to be about 11%, with the actual mass flow rates being under-predicted.

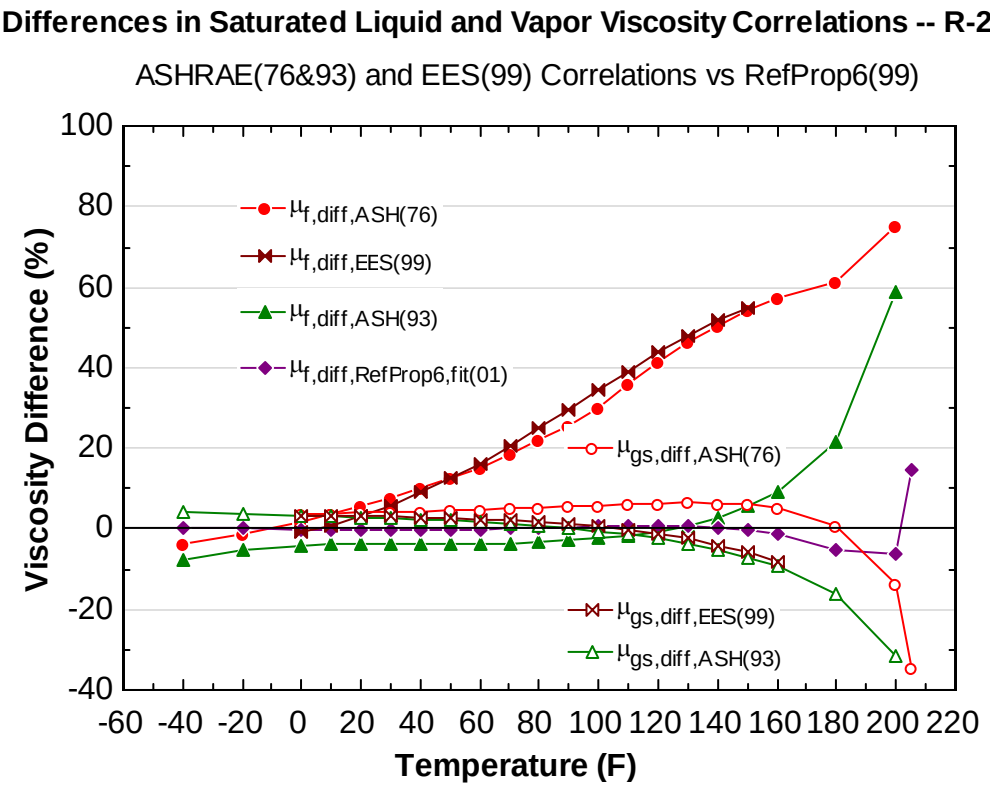

Fig. 10. Percentage differences between R-22 viscosity correlations.

Determination of Capillary Tube Model for Use with R-410A

New Capillary Tube Model For Use with R-410A

We tested and improved ASHRAE-developed capillary tube correlations for R-410A for use with current transport properties. These correlations will be used in planned system analyses comparing high ambient system performance between capillary tubes, short-tube orifices, and TXVs. This work involved refitting the data reported in ASHRAE project RP-762 for both subcooled inlet and two-phase inlet conditions to account for the significant R-410A transport property changes since the data were originally correlated. A plot of the before and after comparisons to test data from RP-762 is shown in Fig. 11. The re-correlated equations match the original ASHRAE test mass flow data almost 10% better than the original when using the transport property data from Geller (2000).

We also tested a less general but property-independent correlation from the same work and corrected a problem with this correlation for inlet quality conditions by refitting the relevant data to the same equation form. (We determined from this that there was a sign error in one of the terms in the published correlation.) We are planning to use the more generalized R-410A correlation in our model but tested the simpler linear alternative as well in case the general model doesn't extrapolate reasonably at higher pressures.

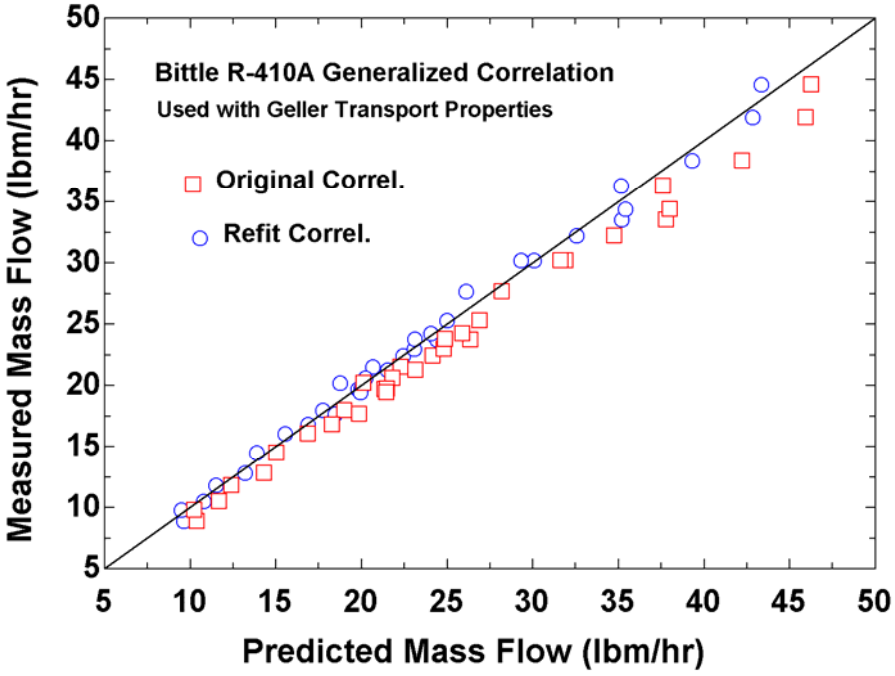

Fig. 11. Comparison of original and revised capillary tube correlations for use with R-410A.

Capillary Tube Model Testing and Implementation

We evaluated two versions of the ASHRAE-sponsored capillary tube correlations for R-410A to decide which to implement in the DOE/ORNL HPDM. The first was the Method 1 correlation for R-410A from ASHRAE RP-762 (1995), and the second was the Method 2 correlation from that report, refitted as described above to adjust for corrected liquid viscosity correlations. These two correlations were also compared to the earlier capillary tube correlation from the 1994 *ASHRAE Refrigeration Handbook* that has been used in the HPDM for many years.

The newer R-410A correlations (in ASHRAE RP-762) were developed over a narrower range of diameters (0.026 to 0.042 in.) and lengths (60 to 200 in.) and for a pressure range of 300 to 420 psia. As the capillary tube size needed for 2 – 3-ton systems (even with multiple evaporator circuits, one capillary tube for each circuit) is 0.05-in. diameter or larger, we compared the correlations at 0.05 in., which was near the upper limit of their intended use.

This comparison is shown in Fig. 12 for subcooling levels of 5 and 20ºF over a range of pressure from 250 to 600 psia. Method 1 is seen to predict a lower effect of both pressure and subcooling on the mass flow rate. Since the Method 2 predictions are more consistent with the previous method and have a refrigerant-property-dependent basis for extrapolation past 420 psia, we chose to implement this approach in HPDM. For capillary tube diameters above 0.05 in., we chose to revert to the existing correlations, which were developed primarily for use with R-12 and R-22.

This limitation of the current ASHRAE correlations to diameters below 0.05 in. and pressures below 450 psia suggests that more test data are needed to extend these correlations to unitary equipment.

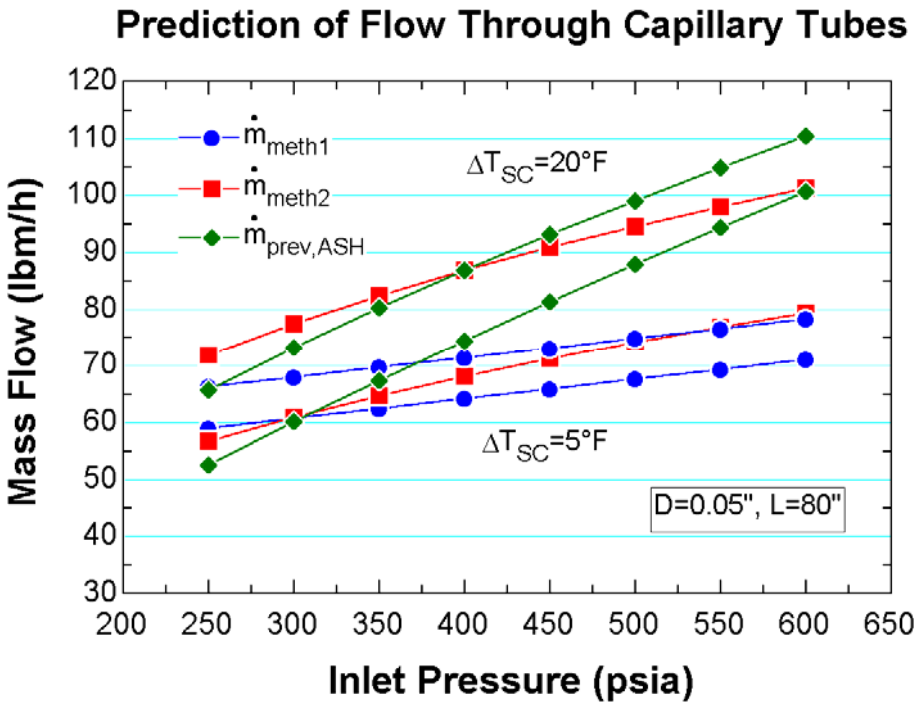

Fig. 12. Comparison of predicted capillary tube flow rates of R-410A using methods 1 and 2 of ASHRAE RP-762 vs. previous ASHRAE Handbook approach.

Improved Compressor Motor Performance Model

In support of the ARTI R-410A extreme ambient projects, Copeland provided single-phase motor performance data for the R-410A scroll compressor used in the NIST tests over a range of voltages from 187 to 253V. This compressor has a nominal hp rating of 2.75 hp and operates at about 135% of nominal hp at the standard 45/130/20°F rating condition.

After comparing this data to what we had available in HPDM (which was based on a three-phase motor of higher slip), we decided to incorporate the new information into our model to provide (1) a better basis for estimating the operating motor speed and efficiency at nominal voltage for the more representative single-phase motor, and (2) a means of adjusting compressor performance maps for over- and under-voltages.

In Fig. 13 and 14, the motor speed and efficiency curves, respectively, of this motor are shown as a function of fractional torque for the three tested voltages at a standard rating temperature. The under-voltage situation is of special interest at extreme operating conditions. As can be seen from Fig. 14, both speed and efficiency fall off more quickly at the more heavily loaded conditions at reduced voltage. This capability allows power draw and EER to be predicted for a worst-case scenario of reduced voltage at extreme ambient temperatures. As a number of the NIST system tests were at less than nominal voltage, we were able to use this model to correct for voltage effects when calibrating and validating our model vs. system performance data.

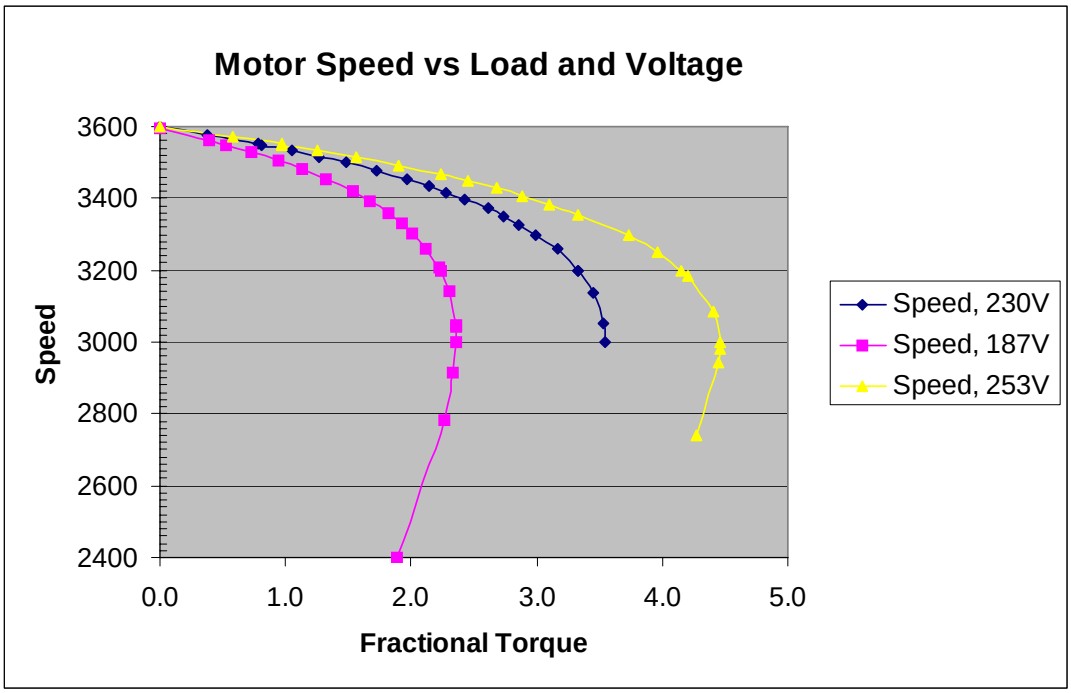

Fig. 13. Motor speed vs. load for the single-phase residential scroll compressor at minimum, nominal, and maximum voltage.

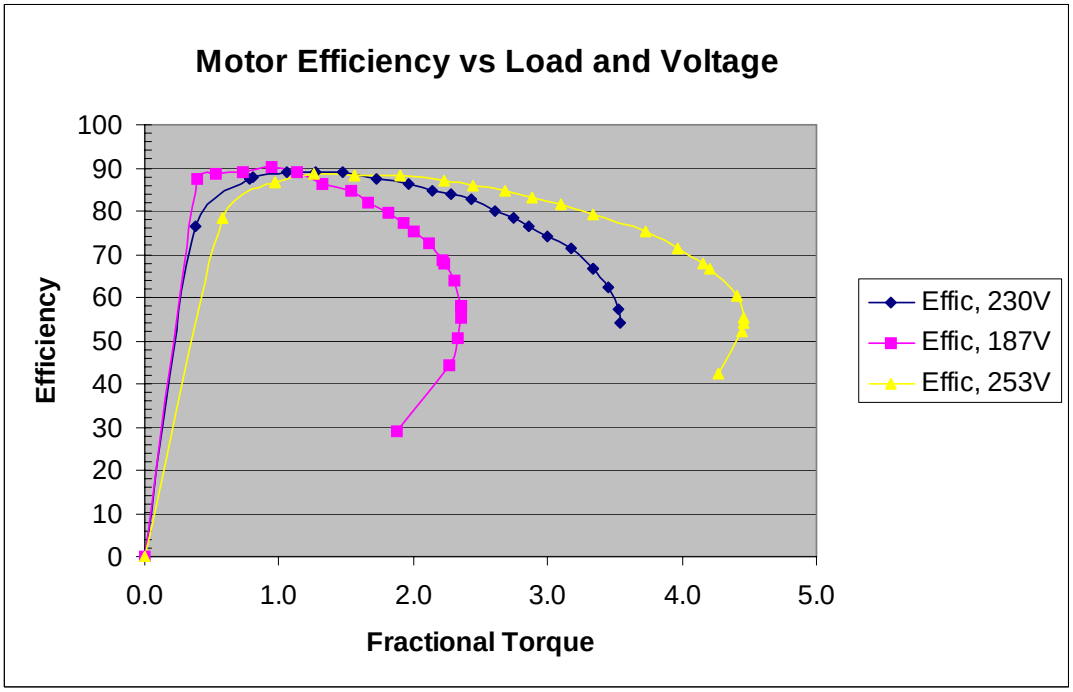

Fig. 14. Motor efficiency vs. load for the single-phase residential scroll compressor at minimum, nominal, and maximum voltage.

Updated Compressor Map Calibration Program

We updated our compressor map tuning program TUNECOMP to work with the compressor motor model, the new compressor map formats, and our most current refrigerant property routines from DuPont. Calculations were also added to determine compressor shell heat loss and loss ratio (as a fraction of compressor input power) from the experimental data for use in specifying shell loss in HPDM. We also added the capability to batch process a set of compressor data over a range of ambient temperatures; this assisted us in determining average heat loss and tuning factors over an ambient temperature range. We used this program with NIST test data to directly determine the required compressor map power and mass flow adjustment factors.

Original and Extended-Range Compressor Performance Maps

In addition to using the compressor performance maps provided by Copeland, we also developed other performance maps for use in the system validation work at ORNL and NIST. We used extended-range (higher condensing temperature) data to develop performance maps as a function of both evaporating and condensing saturation temperatures for sub-critical operation only, and of suction and discharge pressures for use from sub-critical to supercritical operation.

Original and Extended-Range Subcritical Maps

Compressor map coefficients were obtained from Copeland for the R-22 and R-410A scroll compressors used in the NIST test units. In addition, the original data set used to generate the R-410A compressor maps was provided. This data set contained condensing temperatures up to 140ºF and evaporating temperatures up to 55ºF. Copeland's performance tables extrapolate to 150ºF based on this data. From discussions with Copeland about using their maps to predict compressor performance at higher temps, they agreed to run some tests for the ARTI project at higher condensing temperatures up to 160ºF for the R-410A scroll. These data constituted the original and extended-range data sets.

We used the new higher condensing temperature data to obtain extended-range ARI 10-term (and 6-term biquadratic) representations in terms of saturation temperatures for use in near-critical-point analysis. We chose to use the extended data to more accurately predict performance trends near the critical point of R-410A and the outdoor ambient at which the critical temperature is reached. For R-22, we used the standard ARI 540-99 10-term representation (Air-Conditioning and Refrigeration Institute 1999) provided by Copeland.

We generated contour plots to examine the isentropic and volumetric efficiencies for R-22 and R-410A as functions of evaporating and condensing temperatures of most interest to air conditioning application. The R-22 and R-410A results using the original Copeland maps showed trends similar to the R-22 compressor having about 2 – 3 percentage points higher isentropic and volumetric efficiencies over the expected operating region. No unreasonable looking extrapolations were observed for any of these original-range maps. The extended- vs. original-range R-410A maps showed nearly the same isentropic values and trends but different volumetric efficiencies at higher condensing temperatures. The extended map showed less drop-off in volumetric efficiency at elevated ambient temperatures than did the original maps for R-410A and R-22. This suggests that use of an extended-range map for R-410A but not R-22 would likely give R-410A a relative capacity boost at higher ambient temperatures, due primarily to the more detailed data set. So while the extended map is preferred for predicting the point of approach to critical, the original range maps were used for R-410A when comparing to R-22 performance predictions, so as to have consistent representation bias.

Performance Trend Comparisons Between R-22 and R-410A Using Original Maps

In Fig. 2, we showed relative performance trends for R-22 and R-410A up to 160ºF condensing temperature, based on refrigerant property effects alone for fixed refrigerant-side conditions. Figure 15 shows predictions for the R-22 and R-410A test units up to 145ºF ambient (160ºF condensing temperature) — under similar assumptions of constant superheat and subcooling. However, now the evaporating and condensing saturation temperatures differ for the two refrigerants based on the levels they naturally reach in the system (as predicted by the model calibrated against manufacturer's test data at 95ºF ambient) under given ambient conditions with identical heat exchangers. Also, the compressor isentropic and volumetric efficiency variations with saturation conditions are now included. So in Fig. 15, the effects of scroll compressor and HX performance with R-22 and R-410A are included.

While the general performance trends in Figs. 2 and 15 are similar, the equipment performance effects, such as compressor isentropic efficiency drops of 15% at the highest condensing temperatures, cause the relative power to increase more and the EER to drop more than indicated from property effects alone. Thus dropping compressor performance with ambient temperature shifts the absolute trend levels for power and EER considerably and the comparative performance between refrigerants to a somewhat lesser degree.

Figure 16 shows the percentage differences between refrigerant trend lines of Fig. 15.

In Fig. 16, the differences in predicted relative performance between R-410A and R-22 are shown in an AC system with the same heat exchangers and compressor type. The predictions are that, at an ambient temperature of 145ºF where the critical temperature for R-410A is approached, the EER for R-410A will be less than for R-22 by more than 10%, the capacity will be lower by more than 6%, and the power draw will be about 5% higher.

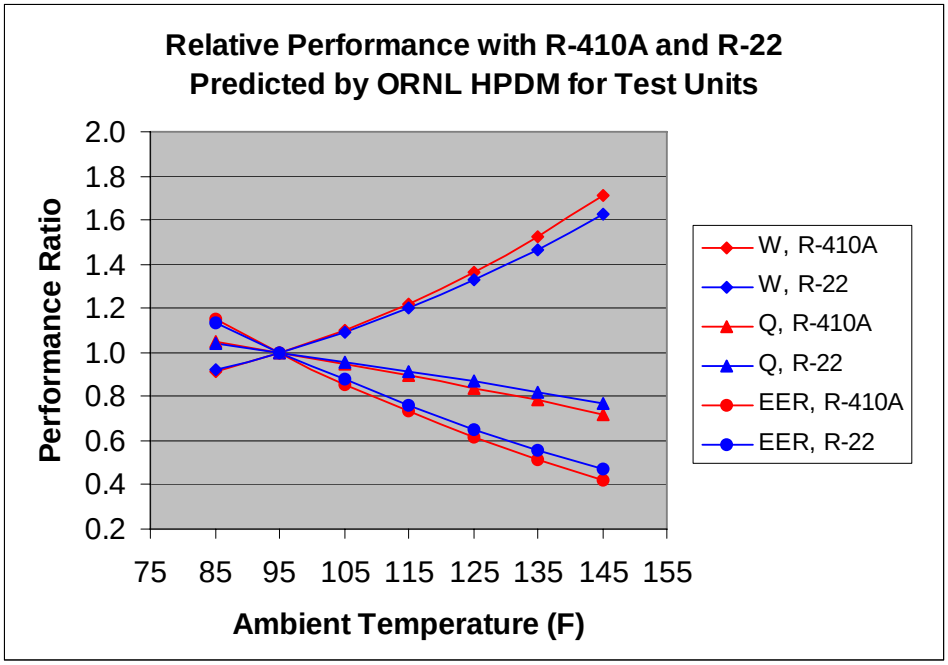

Fig. 15. Predicted equipment performance trends for R-410A vs. R-22 for ambient temperatures up to 145ºF (160ºF condensing) with fixed superheat and subcooling levels — compressor and HX performance effects included, calibrations to 95ºF, manufacturer's data, original R-410A and R-22 maps.

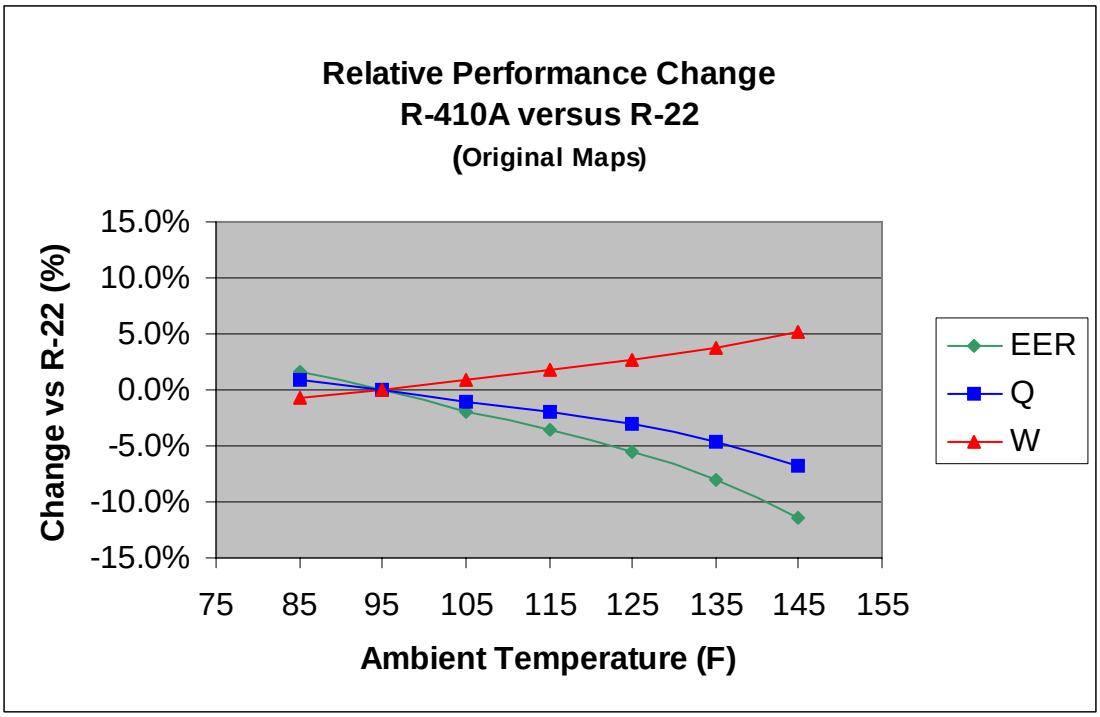

Fig. 16. Relative performance change predicted between R-410A and R-22 for ambient temperatures up to 145ºF (160ºF condensing) in ARTI test units.

If one used theoretical property predictions alone, as shown in Fig. 2 for R-410A vs. R-22, at common saturation temperatures and subcooling and superheat values (of 15 and 10ºF respectively), the EER and capacity loss at the equivalent 145ºF ambient (160ºF condensing) would be predicted at 7.8% and 7.2%, respectively, with a power gain of only 0.8% for R-410A. In Fig. 16, the effects of relative compressor performance result in a higher power draw for R-410A, slightly less drop-off in capacity, with a correspondingly larger drop-off in EER of more than 10%.

Extended Range Maps — From Sub-Critical to Supercritical

Here we used the extended-range data set to obtain pressure-based representations that can be used accurately in both sub-critical and supercritical analyses.

The pressure values for the Copeland data sets we used came from the 1995 Allied-Signal Martin-Hou EOS coefficients (from their Genie program) which we use in the Mark V ORNL HPDM. We determined from discussions with Copeland that this is what was used to set the pressures for their calorimeter tests. So while these pressures are different from those calculated for the same saturation temperature from RefProp6 and our most current EOS, they are the appropriate values for fitting directly to the test data. (From this, it follows that these pressure-based curve fits will be more fundamentally accurate than ones fitted to saturation temperature when used with our newer EOS routines.)

Three map forms available in our heat pump model were evaluated using our MAPFIT compressor data fitting utility program, which was modified to allow curve fits to be obtained to suction and discharge pressure instead of the usual saturation temperatures.

These forms are:

1) a 6-term biquadratic for power and mass flow rate,
2) a 6-term biquadratic for isentropic and volumetric efficiency, and
3) the 10-term ARI 540-99 equation of cubic order for power and mass flow rate.

We used the extended-range compressor data provided by Copeland to test whether efficiency or power/mass flow representations of the standard-range data set ($\leq$140F T_{cond}) extrapolated better to match the extended data (140ºF $\leq T_{cond} \leq$160F). Our previous experience in extrapolating variable-speed compressor data outside limited data set ranges had shown better results with curve fits based on derived isentropic and volumetric efficiencies rather than with raw power and mass flow rate data.

Using the 6-term representations for both approaches, we found, in this case, that curve fits directly to mass flow and power gave better extrapolation results than representations of isentropic and volumetric efficiencies.

We then tried the 10-term ARI 540-99 form and found that the extrapolations were slightly more accurate than with the 6-term biquadratics. So while we are generally dubious about extrapolating with equations such as those used in ARI 540-99 that have cubic terms, this seems to work a little better than the 6-term biquadratics in this case. Since we will not be extrapolating past the extended data set any more than from the 140 to 160ºF saturation temperature range between the standard and the extended data, use of the 10-term ARI equation seemed to be preferable.

Table 1 summarizes these findings based on the maximum deviations.

Table 1. Extrapolation Results Using Standard-Range Data for Compressor Curve Fits

	Maximum error (%)			
Curve — Fit Type	Power	Flow	Isen. eff.	Volum. eff.
6-term efficiency	—	—	–29.0	–8.74
6-term W&flow	–6.71	–6.85	+4.51	–6.85
10-term W&flow	–5.56	–5.47	+3.86	–5.47

Therefore, the following are the proposed compressor performance equations and coefficients for the COPELAND ZP32K3-PFV R-410A scroll unit as a function of suction and discharge pressures.

For power:

COPELAND ZP32K3E-PFV SCROLL, FIT TO STANDARD & EXTENDED DATA
POWER CONSUMPTION (WATTS)
COEFFICIENTS FOR 10-TERM ARI 540-99 CURVE FIT:

F(X,Y)= 1.2900E+03 -1.2716E+01*X + 1.8556E+00*Y +
7.1486E-02*X^2 + 2.0253E-02*X*Y + 5.0362E-03*Y^2 +
-1.6135E-04*X^3 + -4.3825E-05*X^2*Y + -1.3703E-05*Y^2*X +

For refrigerant mass flow rate:

COPELAND ZP32K3E-PFV SCROLL, FIT TO STANDARD & EXTENDED DATA
MASS FLOW RATE (LBM/H)
COEFFICIENTS FOR 10-TERM ARI 540-99 CURVE FIT:

F(X,Y)=-6.3012E+01 3.1245E+00*X + 5.1811E-01*Y +
7.4867E-03*X^2 + -2.6451E-03*X*Y + -1.2426E-03*Y^2 +
-1.8072E-05*X^3 + -3.8133E-06*X^2*Y + 5.4566E-06*Y^2*X +
4.4809E-07*Y^3

X= EVAP. PRESSURE (PSIA)
Y= COND. PRESSURE (PSIA)

The following table shows the results of the 6- and 10-term curve fits using the complete sets of test data.

Table 2. Accuracy of Compressor Curve Fits Using Full Data Range

	Maximum error (%)			
Curve — Fit Type	Power	Flow	Isen. eff.	Volum. eff.
6-term W&flow	– 3.46	– 2.86	4.85	– 2.86
10-term W&flow	– 3.22	1.51	4.09	1.51

We next modified the Mark VI version of our heat pump model to accept the three types of curve fits listed earlier as functions of suction and discharge pressure (as an alternative to saturation temperatures). The new pressure-based curve fit was implemented and found to give predictions for subcritical operation equivalent to the earlier saturation-temperature-based approach.

This completed the modifications needed for the compressor model to handle supercritical operation. These representations, additional details of the pressure-based map fitting analysis, and the compressor map algorithms were provided to NIST per our cooperative working agreement.

SUMMARY OF INFORMATION PROVIDED TO NIST BY ORNL

We used the Mark VI DOE/ORNL HPDM for an early analysis of the sub-critical to near critical operation of the R-410A unit to be tested. The model was calibrated against manufacturer's product data at the 95°F design point, and model predictions were compared to tabulated data up to 115-125°F ambient temperatures. We then ran the program for ambient temperatures > 125°F until a condensing temp of 160°F was reached for R-410A. The ambient temperature of 145°F was identified at which the R-410A unit was predicted to reach critical temperature and this information was provided to NIST. We also ran an alternative way of reaching critical conditions suggested by NIST at the initial review meeting. Here the outdoor ambient was maintained at 135°F and the outdoor airflow was reduced until the critical temperature was approached. A required flow reduction on the outdoor coil from 3150 cfm to between 1550 and 1500 cfm was predicted.

We provided NIST, per our project plans, with compressor map performance correlations as a function of pressures rather than saturation temps, so that they could be used by NIST in their supercritical system performance modeling. Newer extended-range compressor data (at higher condensing temperatures) were obtained and used by ORNL for these performance maps for improved accuracy.

Last, we provided NIST and the ARTI project monitoring committee with early feedback during the lab testing which helped identify and correct some initial measurement issues and problems with compressor power and condenser subcooling levels.

MODEL SETUP AND INITIAL CALIBRATIONS FOR UNITS TO BE TESTED

Initial Modeling and Design Point Calibration

After the first project review meeting, NIST provided us with specific unit and compressor information and some limited product/performance rating data. We obtained further information directly from the system manufacturer for heat exchanger configuration and fin/tubing details as well as product performance engineering data for up to 115°F.

Model Setup

Heat pump model input data sets were assembled for the R-22 and R-410A split system air conditioners to be tested at NIST from information obtained from the system and compressor manufacturers. Both units use the same indoor and outdoor coil and airflow designs. The indoor coil has grooved tubes and the outdoor coil tubes are smooth. Further specifics were obtained this reporting period on the air-side surfaces employed on the coils. Generic air-side surface types were selected (from those available in the model) that were estimated to be most similar to the proprietary surfaces used by the manufacturer. A superslit surface was selected for the evaporator to correspond most closely to the chevron raised lance design, and a louvered surface was chosen for the opposed louver condenser design.

Initial Model Calibration vs. Manufacturer Data

Next, efforts were made to calibrate the model for each unit at 95°F ambient cooling design conditions. The information available for the calibrations is the following:

- design superheat and subcooling levels,
- design pressure drops in the heat exchangers,
- manufacturer generalized charging charts (one average set of conditions for all indoor combinations of each outdoor unit), and
- manufacturer performance data (compressor power, capacity) for the test units from 85°F to 115°F ambient temperatures.

As the refrigerant flow is controlled by TXVs in these units, we modeled their characteristics implicitly (for a properly charged system) by holding superheat and subcooling constant over the range of elevated ambient temperatures. It was confirmed by the manufacturer that this is a close approximation, at least up to elevated ambient levels that they have tested.

Calibration at the design condition was done by adjusting selected compressor and heat exchanger performance multipliers to obtain close agreement on predicted capacity and compressor power. For the compressor multipliers of power and mass flow rate, factors between 0.95 and 1.05 are desirable as this is the allowable test error tolerance for compressor ratings.

Two types of calibration analyses were done. In both cases, we first adjusted the refrigerant-side pressure drop multipliers (and numbers of equivalent circuits, where appropriate) to closely match the expected heat exchanger pressure drops for R-22. Next we tried to match design capacity and power for both refrigerants by adjusting only the compressor multipliers. We were able to obtain good agreement using map multipliers within the ±5% window. However, the predicted evaporating and condensing saturation temperatures were both found to be somewhat higher than that indicated from the charging chart.

We next adjusted the air-side heat transfer multipliers to greater than 1.0 in the condenser and less than 1.0 in the evaporator to more closely approach the saturation temperatures given by the

charging chart. Then we matched capacity and power again by adjusting the compressor multipliers. This time agreement was again reached for the R-22 unit with reasonable map multipliers, but for R-410A, a mass flow multiplier of 1.1 was required and the power multiplier was at the desired upper limit of 1.05.

Even though we had some further issues to resolve with regard to absolute predictions of performance and operating pressures (mainly low-side), we found that relative performance trends, normalized to performance at the 95°F ambient, as a function of outdoor ambient were predicted quite well. Figures 17, 18, and 19 show the predicted vs. manufacturer data for power, capacity, and EER, respectively, for the first calibration approach for R-410A. All performance values have been normalized to those at 95°F ambient. Similar close agreement in trends was found for the R-22 system.

Figures 15 and 16, shown earlier, give the relative performance predicted for R-22 and R-410A as a function of ambient temperatures for the initial calibration to manufacturer's data. Both sets of curves have been normalized to the same performance at the 95°F ambient so that differences in rated performance at 95°F do not confuse the relative performance changes with ambient, which are more of interest in this study.

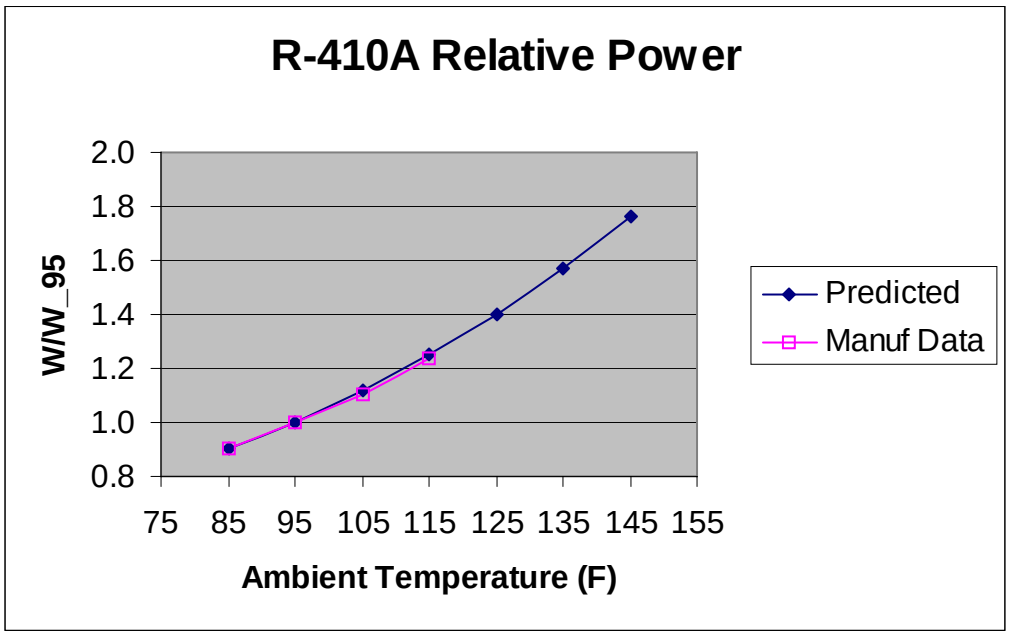

Fig. 17. Relative power trends for R-410A as a function of ambient temperature for initial calibration to manufacturer's data.

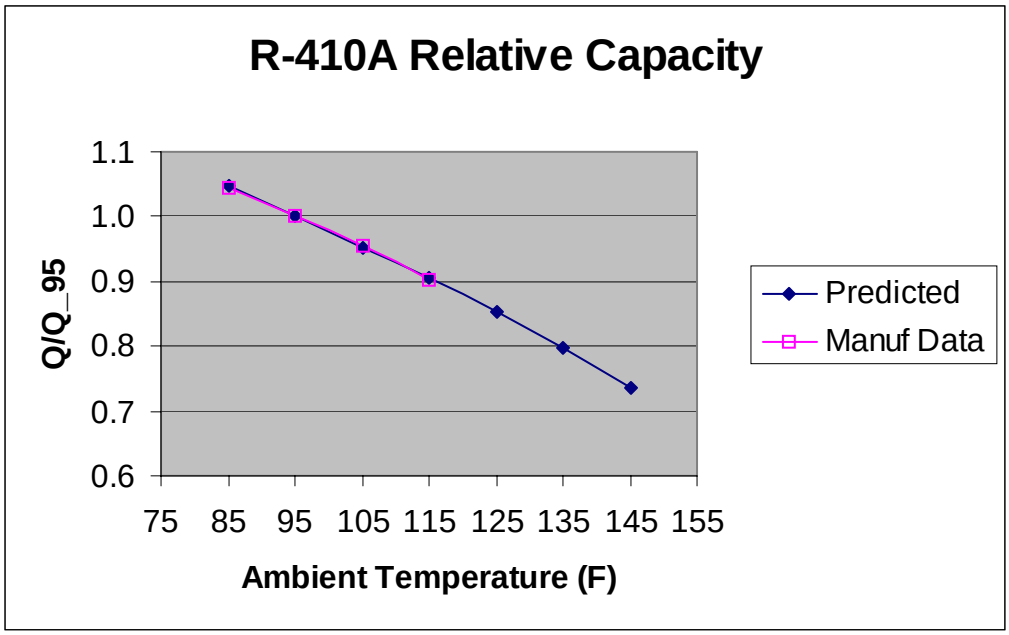

Fig. 18. Relative capacity trends for R-410A as a function of ambient for initial calibration to manufacturer's data.

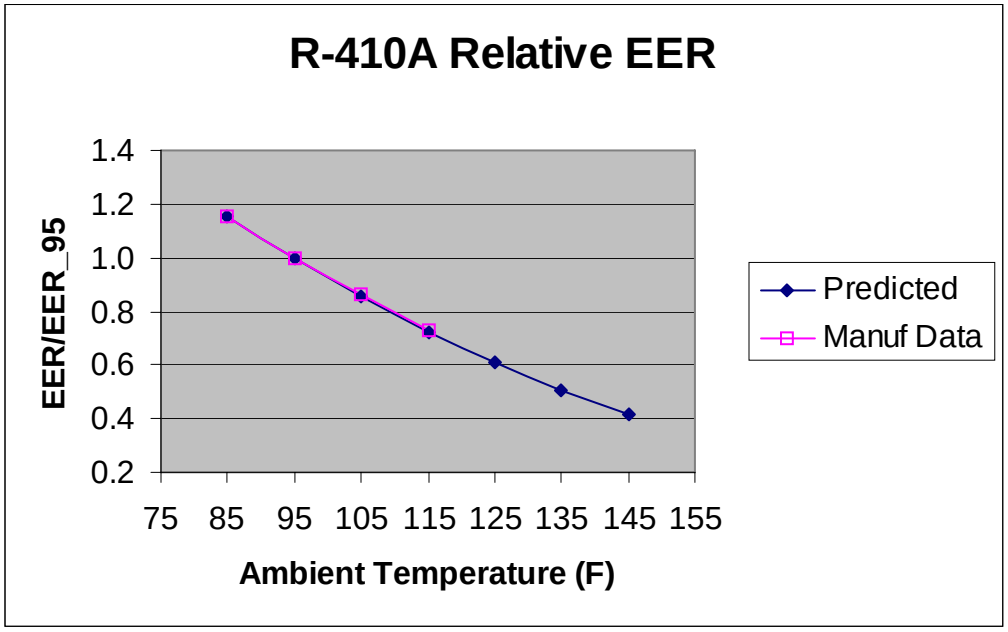

Fig. 19. Relative EER trends for R-410A as a function of ambient temperatures for initial calibration to manufacturer's data.

Further Model Performance Calibrations

Additional manufacturer's performance simulation data were received after the initial calibration work for R-410A and R-22. We used these manufacturer simulations to make additional refrigerant-side comparisons with our improved heat pump model.

Using the updated TUNECOMP program, we determined compressor adjustment factors for each compressor map. For the R-410A case, these were 1.03 for power and 1.01 for mass flow rate at the 95°F design condition, while for the R-22 case they were 1.01 for both power and mass flow.

Adjusting our pressure drop multipliers to match the manufacturer-estimated pressure drops, we found close agreement for the R-410A case. Saturated suction and discharge temperatures were within 1°F with no adjustments in refrigerant- or air-side heat transfer multipliers. The manufacturer-predicted capacity and EER were under-estimated by 2% at this design condition.

For the R-22 case, we over-estimated the manufacturer's predicted evaporating and condensing temperatures by 3.5 and 3°F, respectively. The manufacturer-predicted capacity and EER for R-22 were over-estimated by 5.5 and 4%, respectively. To reach closer agreement, we would have needed to substantially decrease the heat transfer multipliers on the evaporator and increase them on the condenser. We decided to wait for the NIST test data before further seeking to determine suitable calibration factors for the R-22 and R-410A cases.

The differences between manufacturer's R-410A and R-22 simulations were somewhat larger than predicted by our model, with the manufacturer predicting a larger increase in EER and capacity for the R-410A system.

REDUCTION OF NIST TEST DATA

NIST first tested the R-22 system followed by the R-410A system a few months later. We provided early feedback on the initial measurements, helping to identify some power measurement issues and also suggesting additional measurements that were recommended to assist in model validation efforts using refrigerant-side data.

Compressor power measurements were made with both analog and digital meters. After comparing data from both measurements to compressor calorimeter maps over a range of ambient temperatures, we concluded that the digital measurements were the more accurate.

In the initial R-410A tests, using a compressor with the high pressure cutout disabled, as the critical temperature was approached, the OEM compressor failed due to an amp draw higher than the electrical plug was designed to withstand. The compressor manufacturer provided a new compressor with a stronger motor, referred to here as the modified design, as contrasted to the original compressor. This compressor was successfully tested up to and slightly beyond the critical point.

We reduced all of the NIST raw test data for the R-22 and R-410A tests using ORNL-developed EES-based data reduction programs. In these data reduction programs, we calculated saturation temperatures and superheat and subcooling levels at HX exits and compressor and flow control inlets, line pressure drops and temperature changes, and all the usual system performance information such as air- and refrigerant-side capacities. We used the EES program linked with RefProp6 properties to determine these quantities consistent with NIST calculations. For the few tests approaching the critical point, subcooling levels could not be determined with RefProp6 and the DuPont correlations in the ORNL model were used up to the critical point.

Figures 20 and 21 show the calculated subcooling levels leaving the condenser and those entering the flow control for the R-22 and the R-410A tests, respectively. While the subcooling levels leaving the condenser are somewhat lower than that entering the TXV, they are still more than five degrees subcooled in all cases except for a few at 2 to 3°F for the early R-22 test series (designated here as A1). This eliminates the possibility of flashing in the liquid line as a possible reason for the large indicated liquid line pressure drops shown in the previous report. This leaves a clogged liquid line filter or an erroneous TXV inlet pressure transducer as the likely reasons at this point. As far as we know, NIST did not determine that the TXV pressure measurement was incorrect after this issue was raised.

We also calculated the suction line heat gains and the liquid line heat losses as shown in Fig. 22 for the R-22 and R-410A tests. These plots show that all the line heat flows increase significantly with ambient. The liquid line heat losses are the largest, exceeding 2000 Btu/hr at the highest ambient temperatures, being at about the same levels for the different refrigerants. The suction line heat gains, while somewhat smaller, were up to twice as large for R-22 than for R-410A even though the line sizes were the same. Possibly the insulation level was different between the two tests. This higher heat gain resulted in much higher superheats into the compressor for the R-22 tests than for the R-410A. These are shown in Fig. 23.

Heat losses in the discharge line for R-410A were found to be minimal and were not considered further.

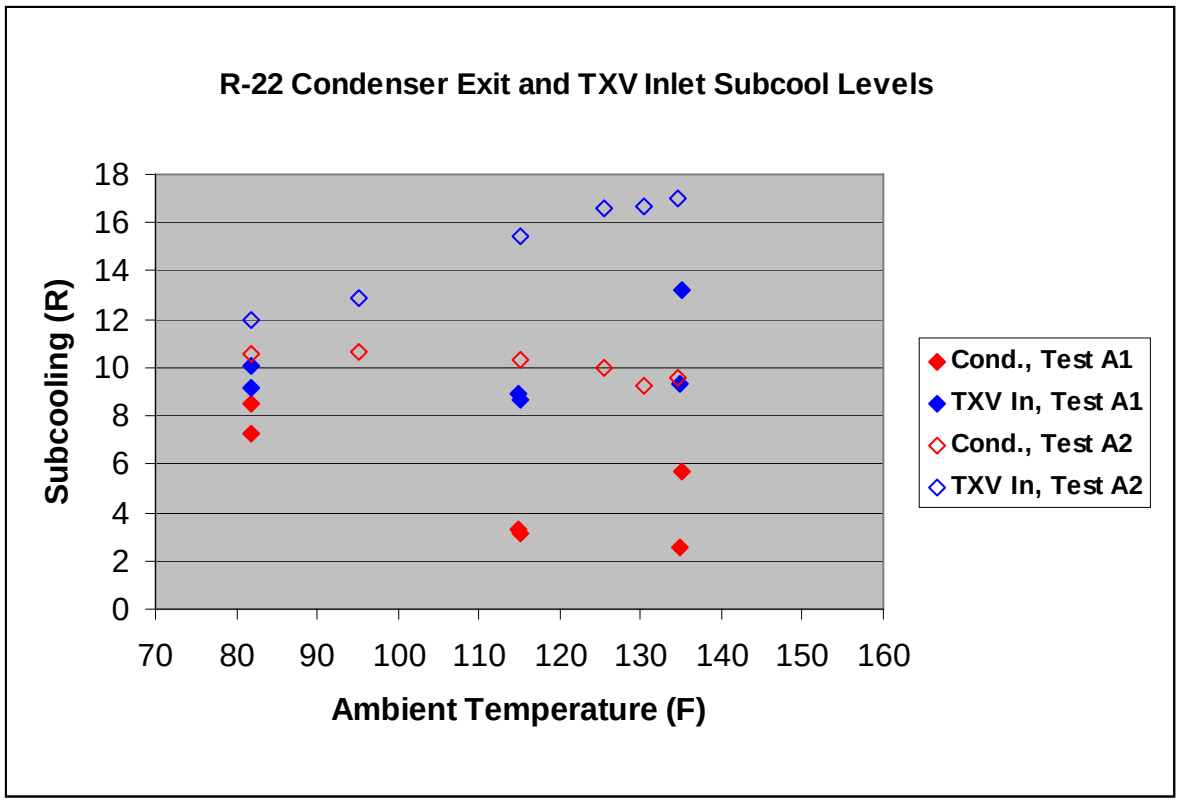

Fig. 20. Calculated refrigerant subcooling levels leaving the condenser and entering the flow control inlet for R-22 tests.

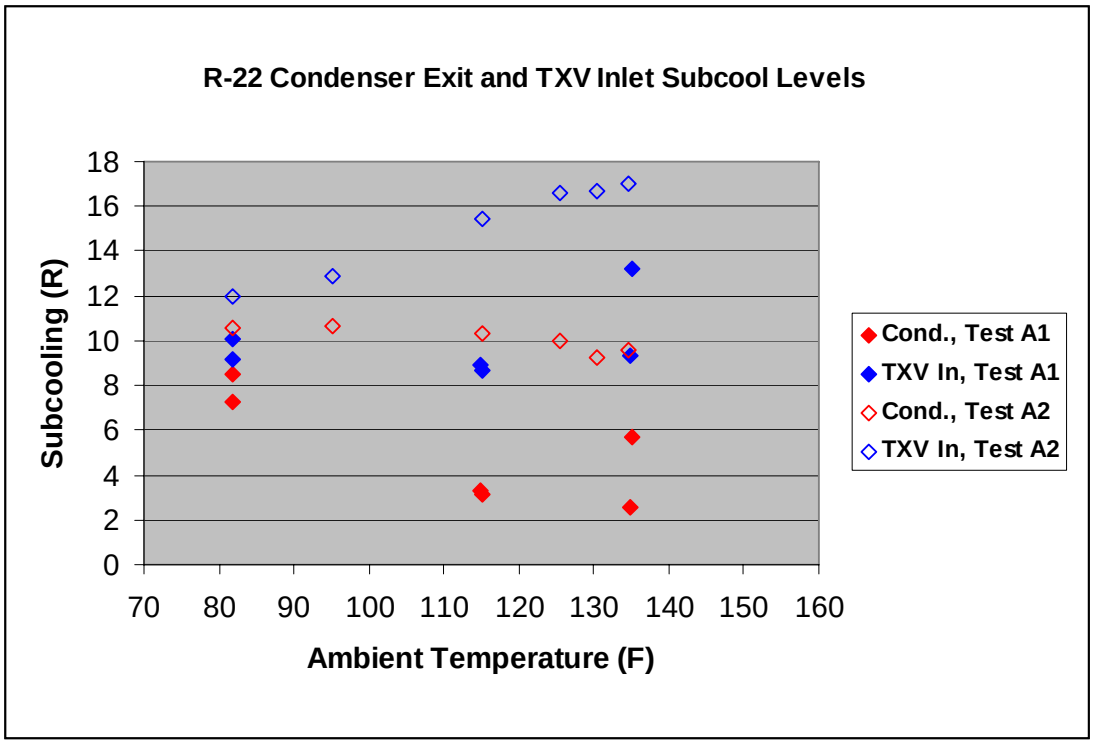

Fig. 21. Calculated refrigerant subcooling levels leaving the condenser and entering the flow control inlet for R-410A tests.

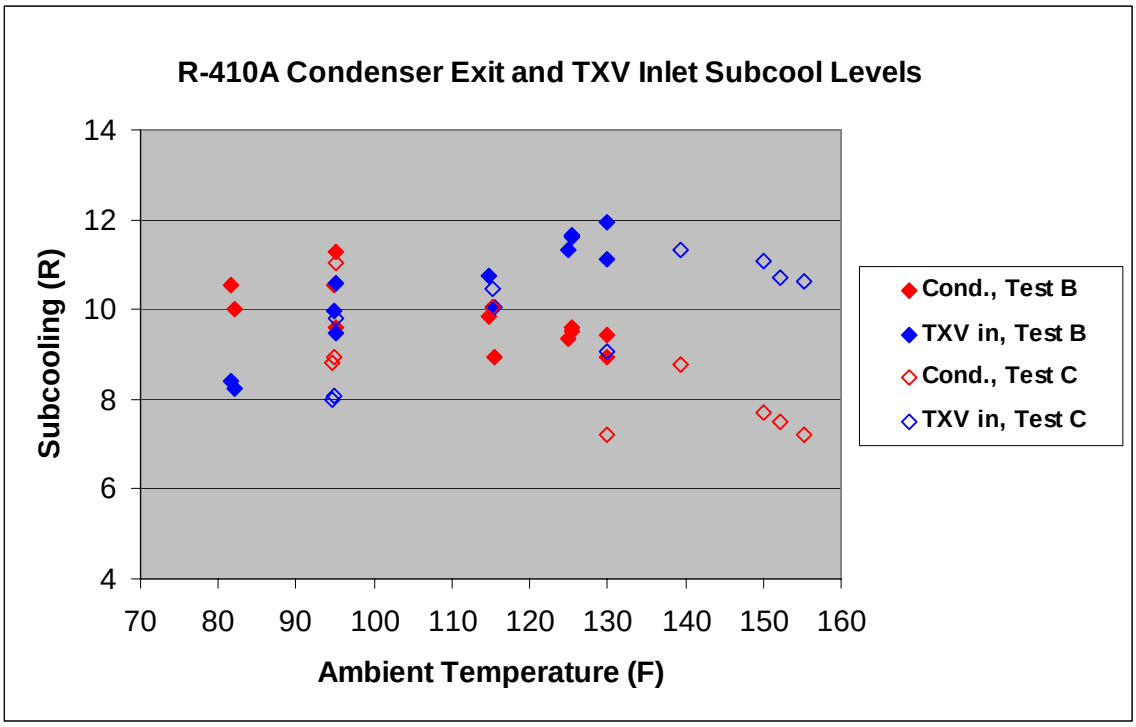

Fig. 22. Calculated refrigerant suction and liquid line heat transfer for R-22 and R-410A tests.

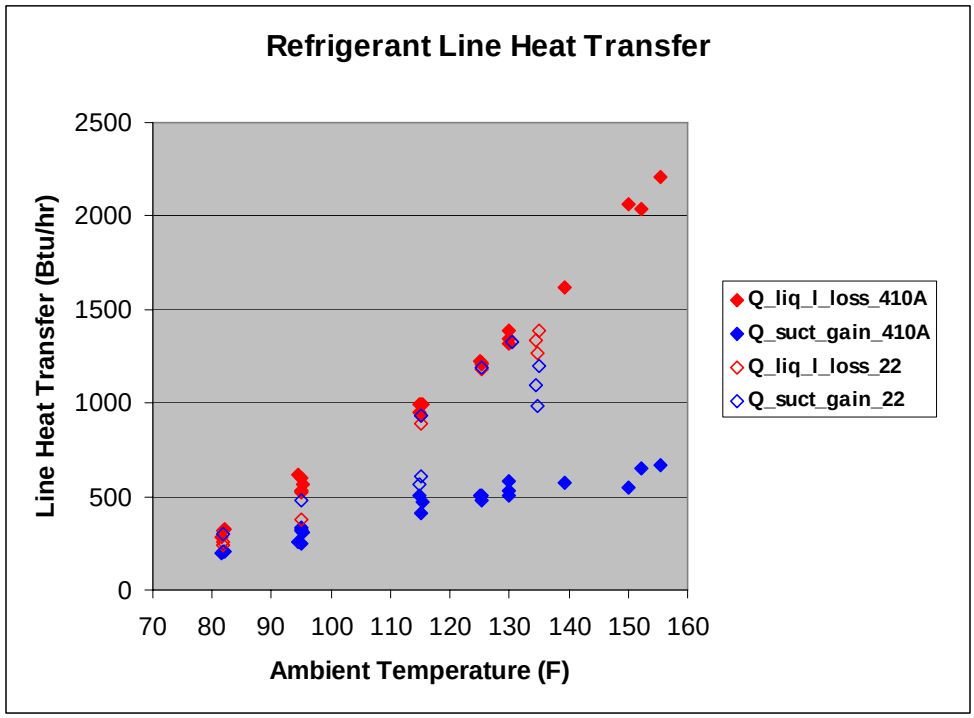

Fig. 23. Calculated refrigerant superheat at evaporator exit and compressor inlet for R-22 and R-410A tests.

In summary, from the reduced data from the R-22 and R-410A tests, we found that the suction line heat gains and liquid line losses increase significantly as a function of ambient temperature. We further found that the *condenser exit subcooling values did not increase with ambient* as it appeared initially. The temperature data we and NIST were both using initially was that for the flow control exit. The additional condenser exit data provided by NIST after our initial data reduction showed that the *HX exit subcooling actually decreases* a couple of degrees *at higher ambient temperatures,* as had been expected previously for a TXV flow control. Significant liquid line cooling at the elevated condenser temperatures caused the TXV inlet subcooling to increase with ambient. The distinction in subcooling trends between condenser exit and TXV inlet was important to determine, as it is important to know where the added subcooling is occurring when calibrating the condenser heat transfer model.

Note that we are using *refrigerant-side capacity* rather than air-side capacity for our EER calculations, as we believe that it is generally more reliable, as well as being consistent with our refrigerant-side validation approach. In general, the agreement between air- and refrigerant-side energy balances for the NIST tests was around 3% at the lower ambient temperatures, increasing to almost 8% at the highest outdoor temperatures. The air-side capacities were always smaller.

In Figs. 24 through 26 we show the measured power, refrigerant-side capacity and EER comparisons for the R-22 and R-410A tests over the tested range of ambient temperatures. The EER values are for the condensing unit, with no indoor fan power effects included since the indoor fan power was supplied externally, in these tests. The plots show that the power draw was the largest and the capacity and thus EER the lowest for the R-410A system with the original compressor. The R-410A system with the stronger compressor (Test Series C) had close to the same EER as the R-22 system with a slightly lower capacity and power draw. These results suggest that use of a larger compressor motor in R-410A systems expected to be in extreme

conditions may be desirable, especially if some means can be provided for nominal compressor shell cooling.

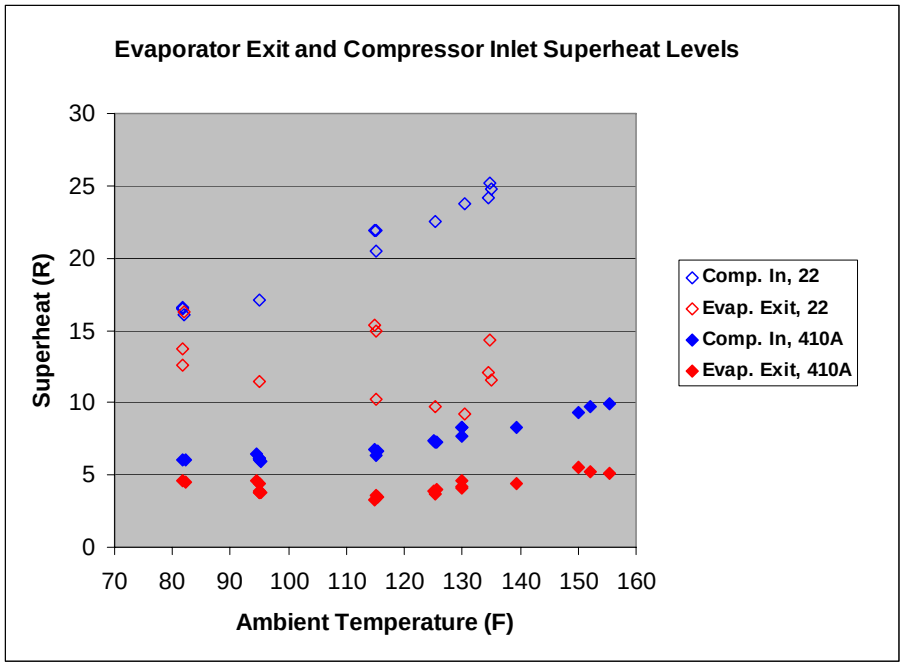

Fig. 24. Measured condensing unit power levels for R-22 and R-410A tests over a range of elevated ambient temperature, no indoor fan power included.

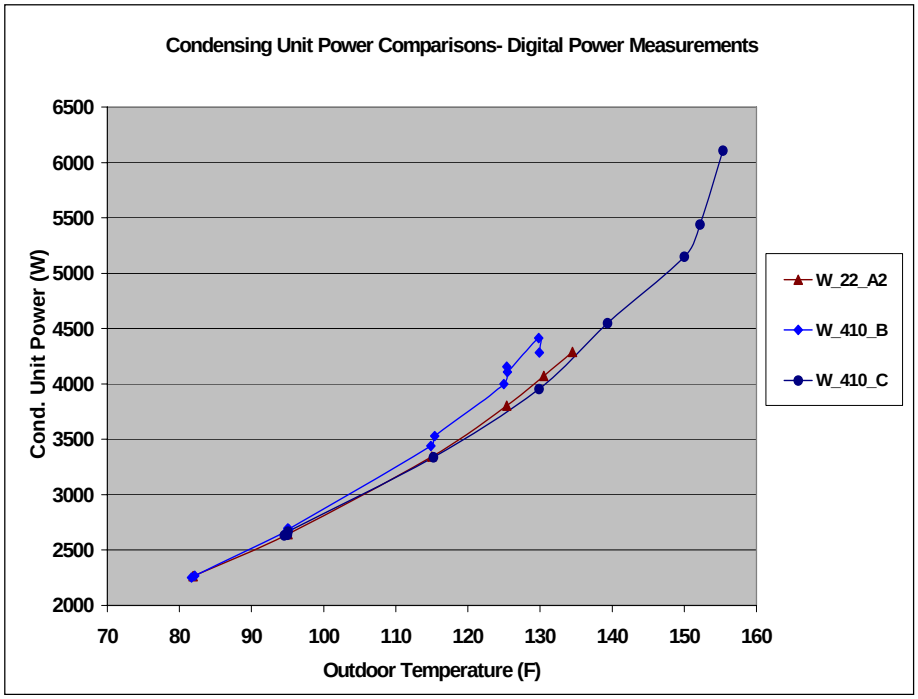

Fig. 25. Measured refrigerant-side capacity levels for R-22 and R-410A tests over a range of elevated ambient temperatures, no indoor fan power effects.

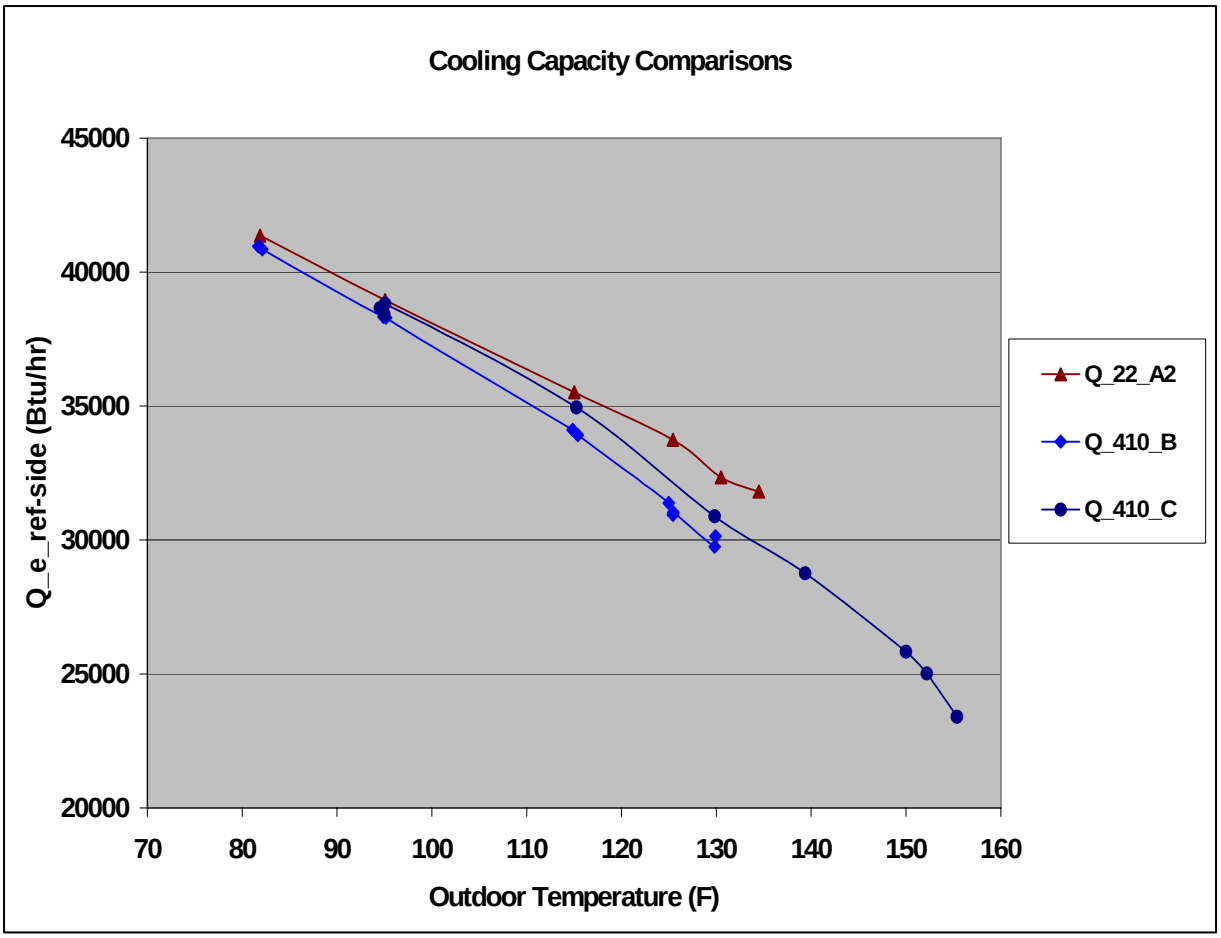

Fig. 26. Measured refrigerant-side EER levels for R-22 and R-410A tests over extended ambient temperature, condensing unit EER, no indoor fan power included.

Compressor Map Calibration Analyses

Analyses were made using our compressor calibration routine TUNECOMP to determine the map adjustment factors that would be needed to bring the compressor map predictions in line with the experimental data.

Power measurements were made by NIST with both watt-hour and digital power meters. The watt-hour meter gave about 5% lower power readings for the R-22 and original R-410A compressor and about 5% higher for the modified R-410A compressor tests. After reviewing all the data, making comparisons to compressor maps at mild ambient temperatures (where the compressor ambients are closest to the map test conditions), and looking at derived compressor shell loss calculations, we concluded that the digital measurements were more consistent and used them in our calibration analysis.

We also determined from discussions with NIST that the compressor input voltage for the system tests was not the standard 230V but rather about 205V for the R-22 and original R-410A tests. The voltage for the modified R-410A test was even lower at 197V. We used the new compressor motor data provided by the manufacturer to correct the compressor map data for mass flow and power. This was done by making corrections for the reduced compressor speed and modified

motor efficiency at the reduced voltages. We found that this adjustment uniformly improved the agreement between the voltage-adjusted compressor maps and the system test data. (Note, however, that making these corrections in the compressor map calibration also assumes that the correct voltages will be provided to the system simulations. Modifications were made to the Web version of Mark VI to allow this to be done.)

The results of our compressor calibration analyses are shown in Figs. 1 – 3 where the required compressor map adjustment factors are plotted for power, refrigerant mass flow, and compressor EER (proportional to mass flow/power), as a function of ambient temperature. Also shown on the plots are the 105% power tolerance and the 95% EER and capacity (proportional to mass flow) tolerances of the ARI 520-90 Standard for compressor testing with a constant 95°F ambient air blowing over the compressor.

In the R-22 comparisons of Fig. 27, the compressor power and EER curves are shown to be in quite good agreement at the lower ambient temperatures. As the compressor maps are developed from data with 95°F ambient air flowing over the compressor shell, this probably corresponds most closely to the 82°F ambient system test, as the compressor sees air at a temperature nearer that leaving the condenser coil. As the ambient temperature increases, clear trends emerge showing increasing correction factors in power while they are decreasing for mass flow and EER. While the map results are in close agreement (<2%) with the R-22 test data for the 82-95°F ambient temperatures, there is a maximum difference of +3% in power and –5% in mass flow at the 135°F ambient test. This gives an EER difference at 135°F ambient of 7–8% lower than the map.

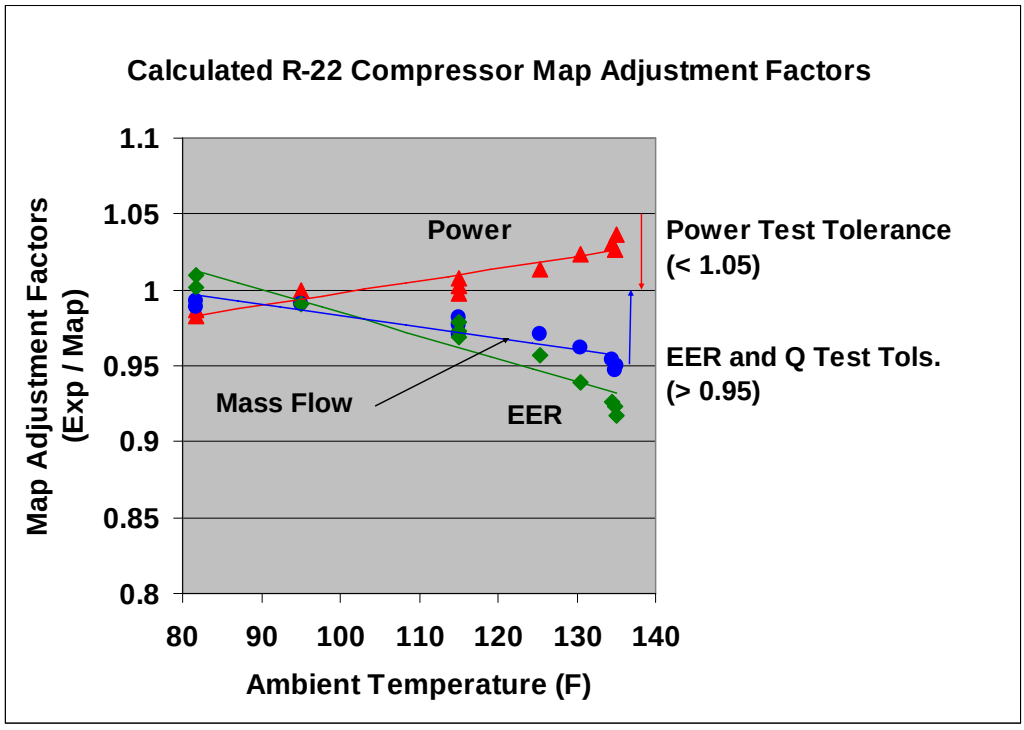

Fig. 27. R-22 compressor map adjustment factor trends for in-situ compressor performance at elevated ambient temperature.

In Fig. 28, we show comparable results for the original R-410A compressor tests after making the voltage corrections to the map. Note that we used the extended-range compressor map for R-410A, which would be expected to provide better representation of performance at elevated ambient temperatures than the standard map used for the R-22 compressor. Here again the agreement in mass flow rate and power are excellent at the 82°F condition; however, at higher ambient temperatures the R-410A data begin to deviate more quickly and more widely from the corrected map than for the R-22 case. At the maximum 130°F ambient tests, the power deviations are up to +7.5%, mass flow drop-offs at –7.5 to –9%, with EER deviations up to –15%.

Map comparisons for the R-410A C-Test Series with the modified compressor (stronger motor) are shown in Fig. 29, where the same extended-range compressor map (for the original motor) was again used. Here, correction of the map to 197V conditions results in agreement to within 3% in all measurements below 130°F ambient. Only near 140°F and beyond are the mass flow and EER values more than 5% low. The power corrections show a slight trend downward until 150°F ambient, in contrast to the other compressors, and then begin to rise, remaining less than 5% for all but the highest ambient.

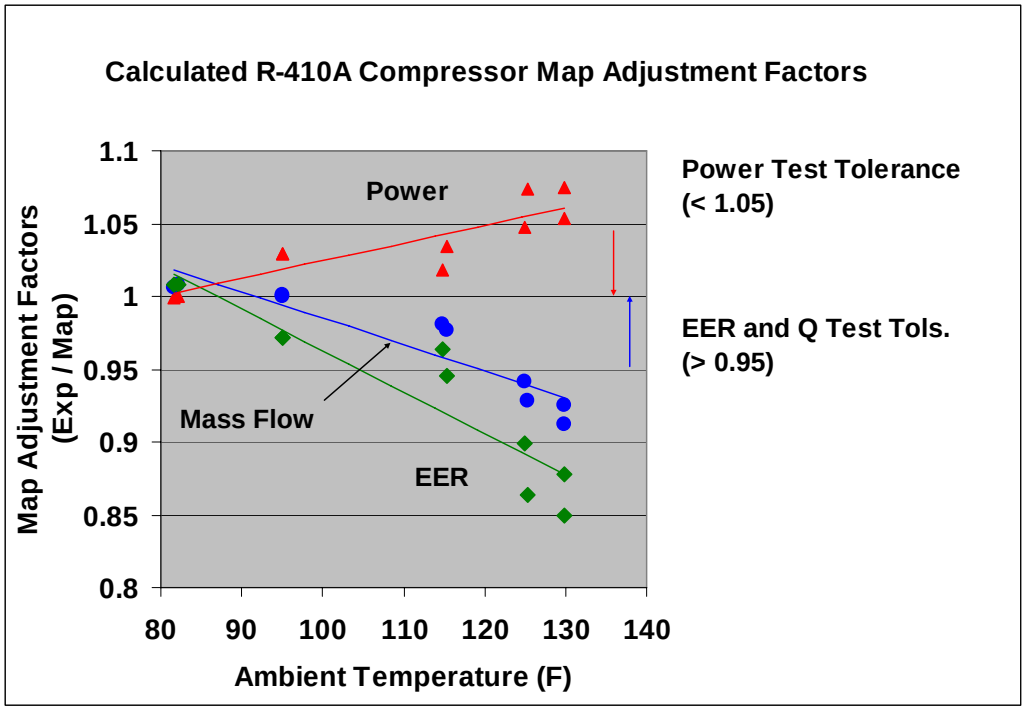

Fig. 28. Original R-410A compressor map adjustment factor trends for in-situ compressor performance at elevated ambient temperature.

These results show that for all three compressors, there is generally quite close agreement at mild ambient temperatures using the digital meter power data. At higher ambient temperatures, there is a consistent loss in mass flow rate (and thereby in capacity) capability for all three compressors. For the original R-22 and R-410A scroll compressors, there is also a clear trend of increased power use relative to the map at higher ambient temperatures, more so for the R-410A compressor. The original R-410A compressor loses the most performance at elevated ambient temperatures.

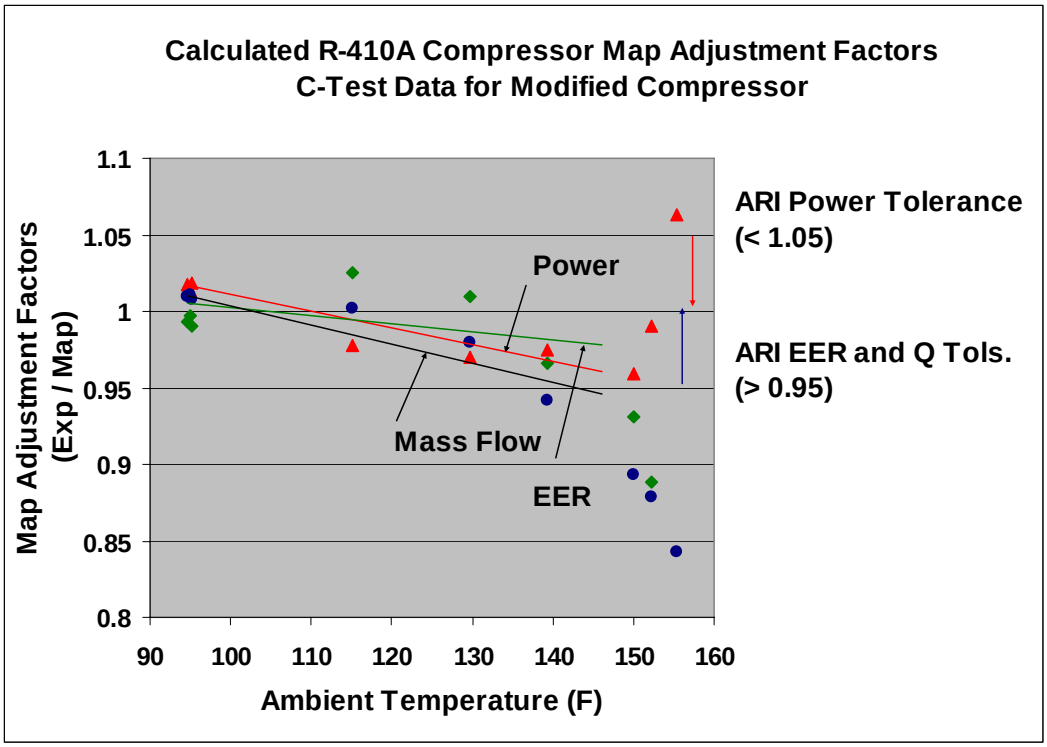

Fig. 29. Modified R-410A compressor map adjustment factor trends for in-situ compressor performance at elevated ambient temperature.

This suggests to us that the motor performance is dropping at these conditions due to the elevated motor temperatures as compared to the compressor test standard (ARI Standard 520-90) with the 95°F air-over conditions. A reduction in motor speed and an increase in power draw would be expected effects of higher motor temperatures. (The corrections in our model for reduced voltage are based on motor tests at room temperature, so would not account for these added motor temperature effects.) It appears that the original R-410A motor may be undersized relative to the R-22 motor, based on the suction, discharge, and compressor shell operating conditions that it is seeing under elevated ambient temperatures.

Typically, we have used one test point at the 95°F design condition to calibrate the compressor map to field conditions. Here, the data suggest that a function with ambient temperature is needed to better make the needed adjustments. In fact, if only one calibration point were to be used, it should probably be at the most elevated ambient test available with a zero correction applied at 82°F. Our system model was modified to use variable adjustment factors based on this calibration analysis. Straight-line approximations to these adjustment factors were obtained for each compressor for use in the system validation tests.

Compressor Performance Analysis

Relative Compressor Performance. Figures 30 – 31 show the overall isentropic and volumetric efficiencies for all three compressors tested over the range of ambient temperatures. These figures show that with a stronger motor, the R-410A compressor performs nearly the same as the R-22 compressor at higher ambient temperatures, even with the reduced voltage, although starting out lower in mild ambient performance. These results show that the stronger motor significantly improved the high ambient temperature performance of the R-410A compressor.

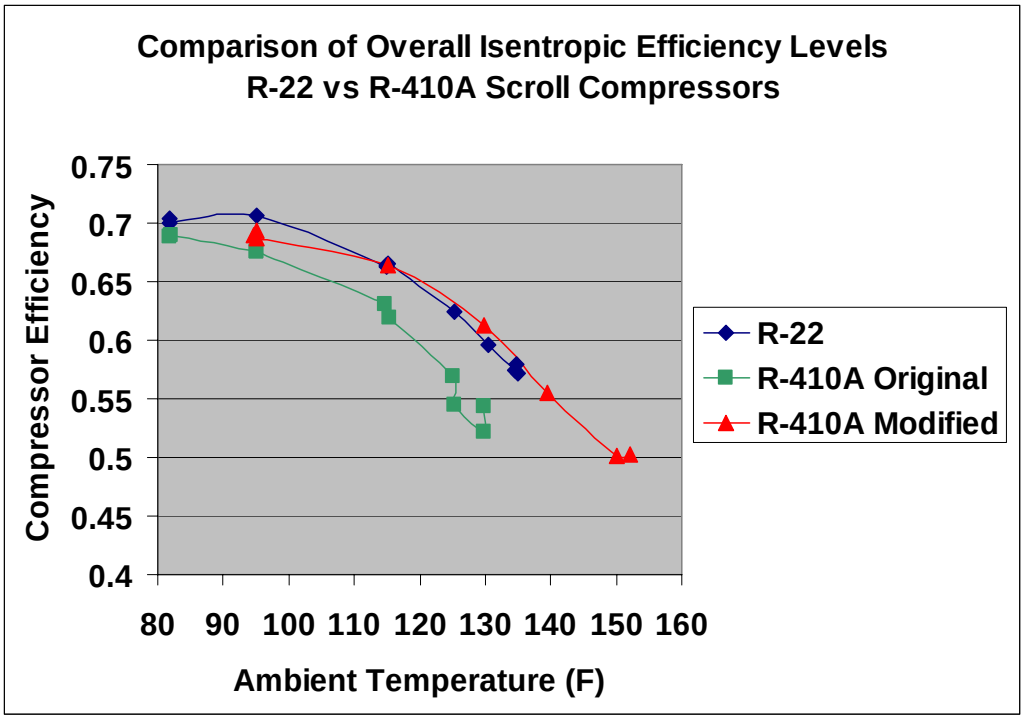

Fig. 30. Comparison of compressor overall isentropic efficiencies for three compressors tested in-situ by NIST — digital power measurement.

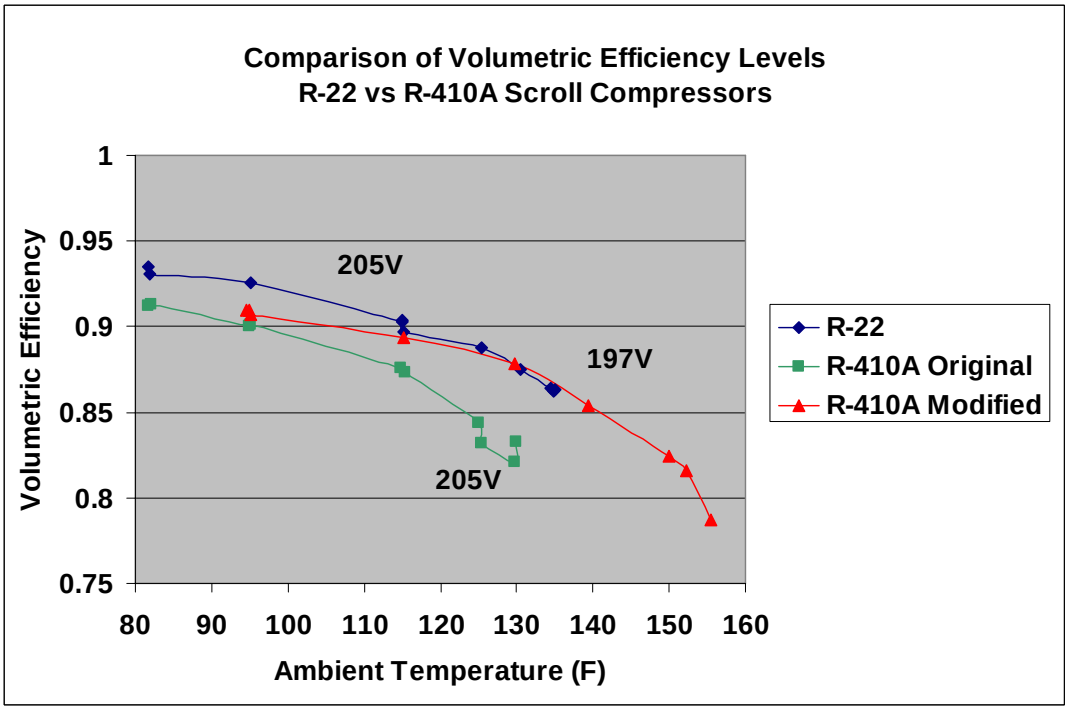

Fig. 31. Comparison of compressor overall volumetric efficiency for three compressors tested in-situ by NIST.

Compressor Shell Heat Loss Fraction

We also looked at compressor shell heat loss as a fraction of input power, since an estimate of shell heat loss is needed by the system model to calculate accurate compressor discharge temperatures. Because shell heat loss is determined by an energy balance on the compressor (as power in — energy supplied to the refrigerant), heat loss fraction is another useful way to judge the reasonableness of measured compressor data (including discharge temperature). We used this approach to help determine that the digital power measurements were more consistent than the analog measurements.

Further Analysis of Compressor Performance Losses at Higher Ambient Temperatures

As a follow-up to the compressor map performance calibrations, we compared the compressor shell heat loss in system tests to those from manufacturer's calorimeter tests and found a 50% reduction. This finding helps to explain the lower compressor performance relative to the map.

In trying to better understand drops in compressor performance at higher ambient temperatures found in the compressor map comparisons, we went back to the extended-range R-410A compressor tests done by the manufacturer. Using the measured discharge temperatures, we calculated shell heat losses for the calorimeter tests with 95°F air blowing over the compressor at 1360 cfm. This compares to the outdoor unit test configuration where the compressor was not in the air stream but off in a separate compartment seeing approximately ambient air temperature. (In the tests, the cover was off the box so the compressor was cooler than it would have been in an actual field unit. This implies that the field performance drop-off might be larger than seen in the system tests.)

A comparison of the shell heat loss fractions (of compressor input power) in the calorimeter tests of the original R-410A compressor to those in the unit tests is shown in Fig. 32. This shows that the heat losses were reduced by at least 50% in the test unit until condensing temperatures

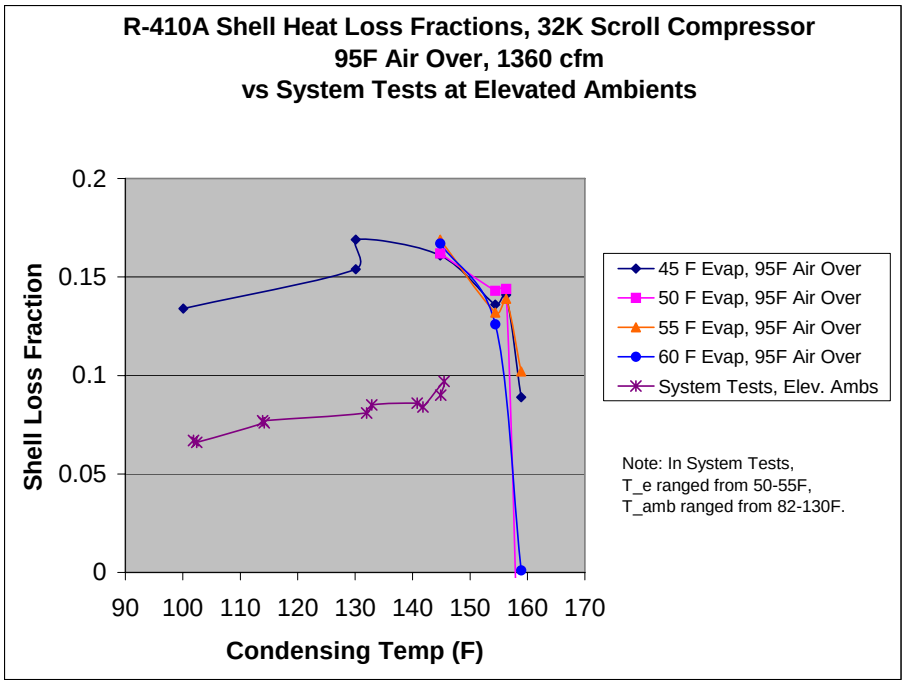

Fig. 32. Comparison of compressor shell heat loss fractions between calorimeter and system tests for original R-410A compressor.

exceeded 140°F. This reduction appears to be mainly due to reduced airflow over the compressor, as the effect of ambient changing from 82°F to 130°F in the system test gives a shell loss trend about the same as for the calorimeter test where the ambient was held at 95°F. This reduction in external heat loss would cause the suction gas to be further superheated before entering the suction port and the motor to run hotter. These effects would be consistent with a loss in mass flow and increase in power draw relative to the calorimeter results as shown in the last report.

Above 150°F, the calorimeter-tested compressor is rejecting less and less of the input power, until above 155°F, it appears that thermal equilibrium was lost and the compressor exit was hotter than could be accounted for by a steady-state energy balance, i.e., the compressor body was heating up. This suggests that in the system tests, the reduced airflow over the shell may have contributed to the overheating of the power plug in the compressor that failed.

In general, these findings suggest that modeling of systems at elevated ambient temperatures will be improved if reliable information is available to correct compressor performance for reduced airflow and/or elevated ambient effects. Without such corrections, the power will be under-estimated and the capacity and EER over-estimated to an increasing degree with higher ambient temperatures. A common compressor location is below the outdoor fan at the condenser exit. Here the compressor is in the airflow, but air temperatures can be much higher than 95°F and the compressors may be insulated to varying degrees.

We did not have sufficient information on the R-22 compressor to calculate the shell heat loss for the standard compressor map tests for comparison.

A comparison of the shell losses for all three compressors based on digital power measurements are shown in Fig. 33. From the data, we determined that a specified shell heat loss fraction value that varies with ambient would be useful for the system modeling.

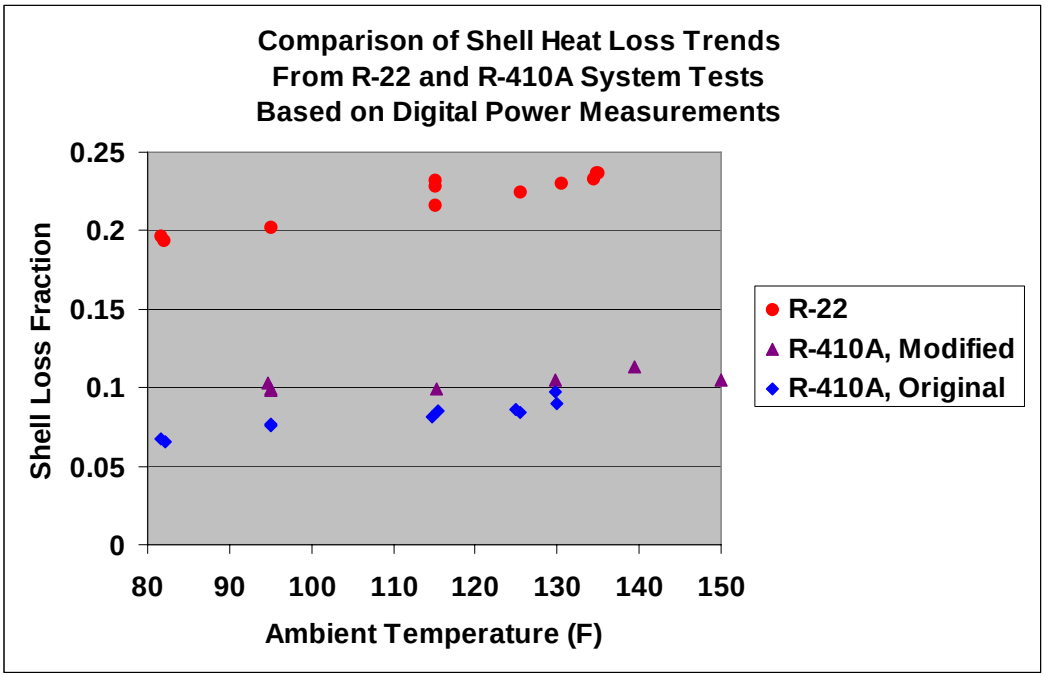

Fig. 33. In-situ compressor shell heat loss fractions for the three compressors tested at NIST.

MODEL CALIBRATIONS TO NIST TEST DATA

Our model was calibrated against the NIST R-410A data (NIST 2001) to match the measured heat exchanger pressure drops and manufacturer-estimated air-side heat transfer coefficients. Because the heat exchanger pressure drops were uncertain for the R-22 tests due to measurement problems, we could not separately calibrate the HX pressure drop model, so we used the R-410A HX pressure drop calibration factors. Extra liquid line pressure drops, larger for the R-410A case than for the R-22 case, had to be added to better match the TXV inlet conditions. (These added pressure drop values change with the square of the flow rate in our program.)

The required adjustments to the generic heat transfer coefficients for the louvered and slit-fin surfaces to match the manufacturer's estimated values were quite small (less than 10%). In contrast, the pressure drop multipliers needed to match the measured R-410A values were quite large (about 3), indicating that the present models do a poor job of predicting absolute levels of pressure drop for these heat exchangers, perhaps due in part to the effects of oil in the evaporator and because of the approximate nature of the circuitry treatment in the condenser.

These calibrations improved agreement with measured refrigerant-side conditions over previous efforts for R-22 but still left some unresolved differences in low- and high-side saturation temperatures. Generally, the model predicted lower evaporating and condensing saturation temperatures relative to those derived from measured pressures for both R-22 and R-410A systems. The difference in evaporating temperatures (–1.9 to –2.8°F) was larger than in condensing (–0.7 to –1.0°F), and larger for R-22 systems than for R-410A in the evaporator (–2.8°F vs. –1.9°F), but smaller in the condenser (–0.7°F vs. –1.0°F) . The sensible heat ratios predicted by the model were also higher than found in the tests (0.77 vs. 0.72). Attempts to raise the evaporating temperature by increasing the air-side heat transfer coefficient resulted in larger discrepancies in sensible heat ratio values and so were not pursued further.

As a result of the lower evaporating temperatures, the predicted cooling capacity and EER levels are about 5% low for the R-22 system and 2–4% lower for the R-410A cases. Agreement is within 1% for R-410A and 2.5% for R-22 if air-side capacities and EERs are used.

It appears that the lower predicted evaporating temperatures are the driver for the differences in capacity and condensing temperature. This is because the lower evaporator pressure causes the refrigerant mass flow and therefore the condenser loading and condensing temperature to be lower than in the experiment.

MODEL MODIFICATIONS RELATED TO OFF-DESIGN SIMULATION

After we determined from the test data reduction analysis that significant corrections were needed to the compressor and line heat transfer losses, we added to our system model the capability to specify compressor map power and mass flow adjustment factors, compressor shell heat loss, and suction, discharge, and liquid line heat transfer as a function of ambient temperature. This allows us to specify these varying quantities with ambient temperature along with the compressor inlet superheat and condenser exit subcooling in our model validation tests.

These capabilities were implemented in the Web version of the Mark VI HPDM and made available online at www.ornl.gov/~wlj/hpdm/MarkVI.shtml. These are accessible from the Parametrics Analysis calculation path as ambient control options under the Outdoor Air Inlet Temperature parametric selection.

With these model additions, we completed the calibration and validation analyses using NIST test data up to within a degree of the critical point.

FINAL MODEL VALIDATIONS

The ORNL HPDM was next set up to run from 75 to 145°F for three validation cases — R-22 tests (test series A2), R-410A tests with original compressor (test series B), and R-410A tests with the modified compressor (test series C). (The condenser saturation temperatures for the R-410A cases were just below 160°F at the 145°F ambient condition.)

We used experimental data for each of the three test series [A2 (R-22), B and C (R-410A)] to specify linear variations in:

- compressor inlet superheat,
- condenser exit subcooling,
- suction line heat gain,
- liquid line discharge loss,
- compressor shell heat loss, and
- compressor map mass flow and power adjustments,

as functions of ambient temperature, employing the newly added parameter-variation capabilities. For the R-22 tests, we used the later tests (designated A2) with the higher subcooling levels as the basis for these values.

Figure 34 shows an example of the relationship used for representing condenser subcooling for the R-22 vs. R-410A analyses.

In Figs. 35 and 36, we show respectively the measured and predicted compressor inlet and exit saturation temperatures for R-22 vs. R-410A. It can be seen that the model predicts larger differences in saturation temperature, especially on the suction side, between R-22 and R-410A than are seen in the experiment.

In Figs. 37 and 38, the model predictions for refrigerant-side pressure drop are compared to the directly measured values for R-410A and the estimated values for R-22. (The estimated R-22 condenser pressure drop values were based on measured total high-side pressure drop and estimated liquid line pressure drop, which varied with flow ratio squared. The estimated R-22 evaporator pressure drop was simply the predicted value at 95°F ambient, again varied by the flow ratio squared.) For R-410A, measured data and predictions for both compressor tests are combined.

The model-predicted pressure drops are based on Martinelli-Nelson/Thom correlations, generalized from steam to other fluids by a property index based on liquid-to-vapor density ratio as discussed by Goldstein (ASHRAE 1979).

From the R-410A comparisons in Fig. 37, it can be seen that the model does not predict the measured increase in evaporator pressure drop at higher ambient temperatures. However, in the condenser, the model predicts a slightly larger change in pressure drop with ambient than measured.

With the R-22 comparisons in Fig. 38, a similar but even stronger trend is seen in the condenser where the model seems to over-predict the pressure drop at mild ambient temperatures and under-predict at elevated ambient temperatures. In the evaporator, the estimated values are based on the simple flow rate dependence which matches closely the nearly constant predicted values.

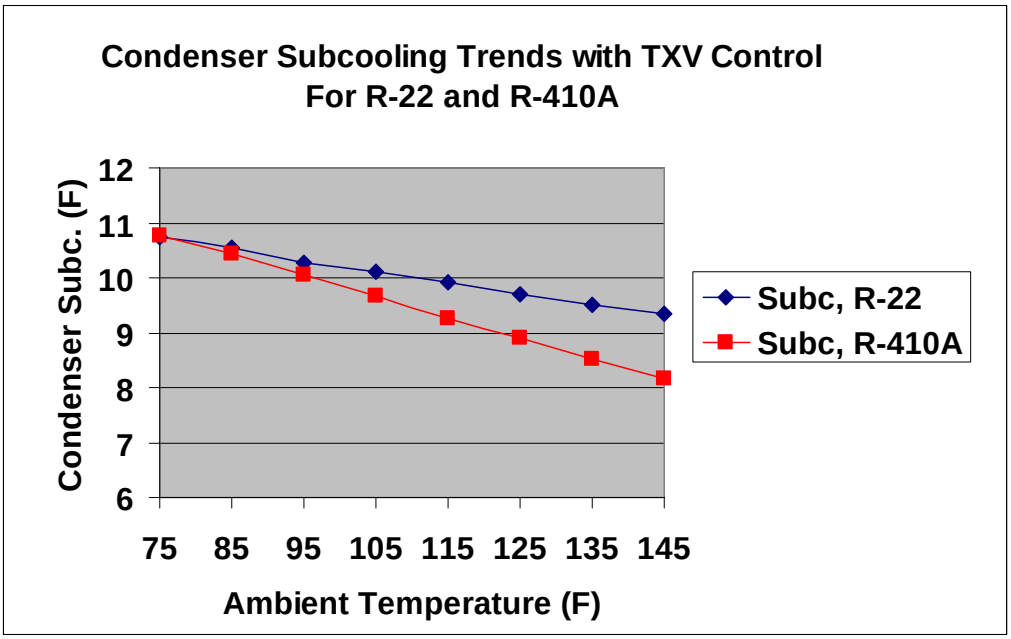

Fig. 34. Subcooling trends with ambient based on NIST testing as used in ORNL system simulations for R-22 and R-410A.

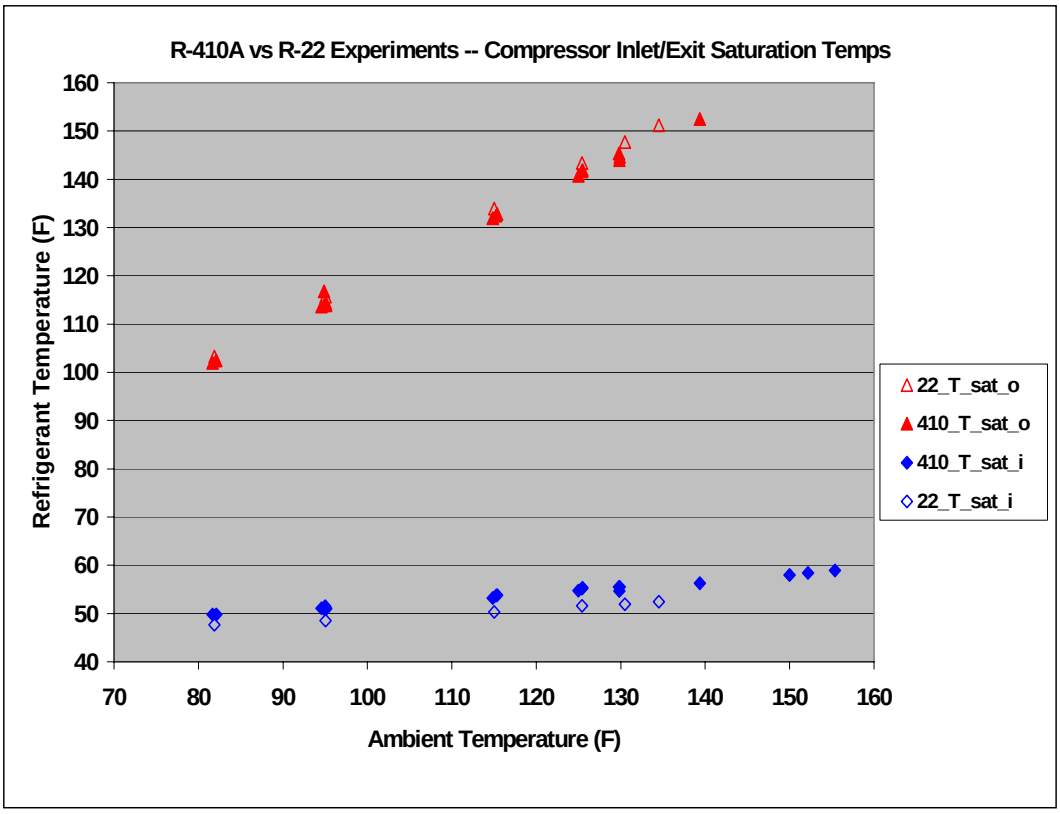

Fig. 35. Experimental saturation temperatures at the compressor inlet and exit for R-22 vs. R-410A over a range of elevated ambient temperature.

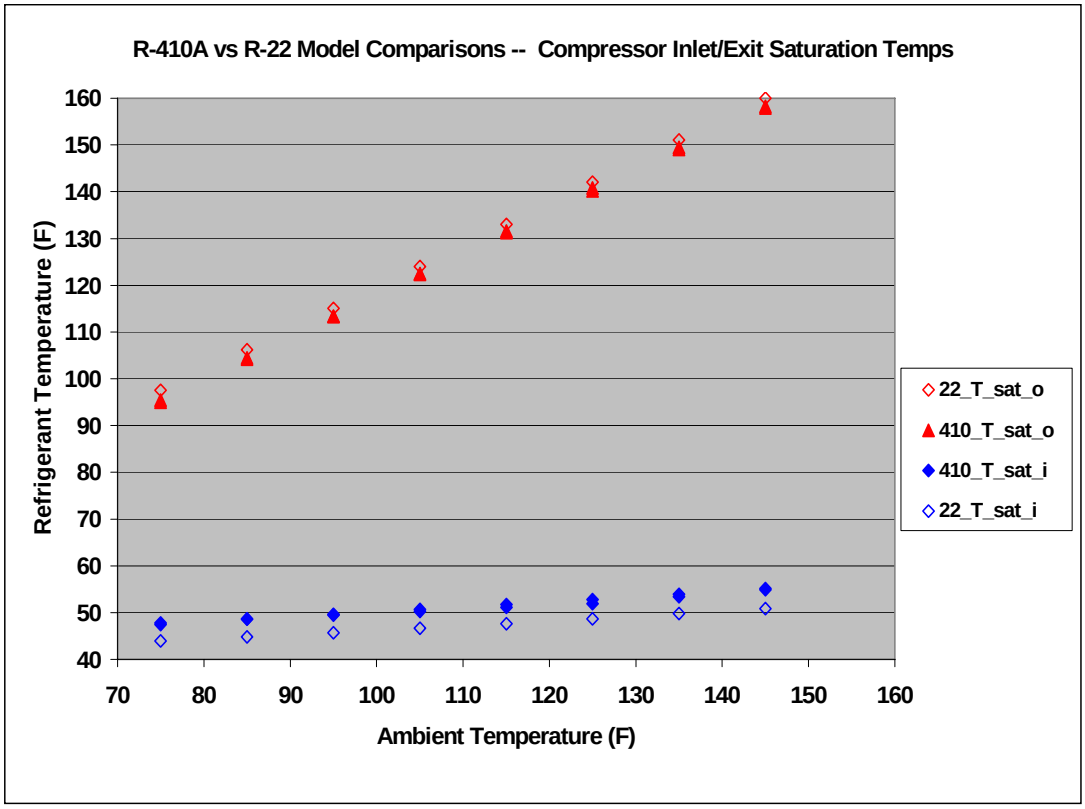

Fig. 36. Predicted saturation temperatures at the compressor inlet and exit for R-22 vs. R-410A over a range of elevated ambient temperature.

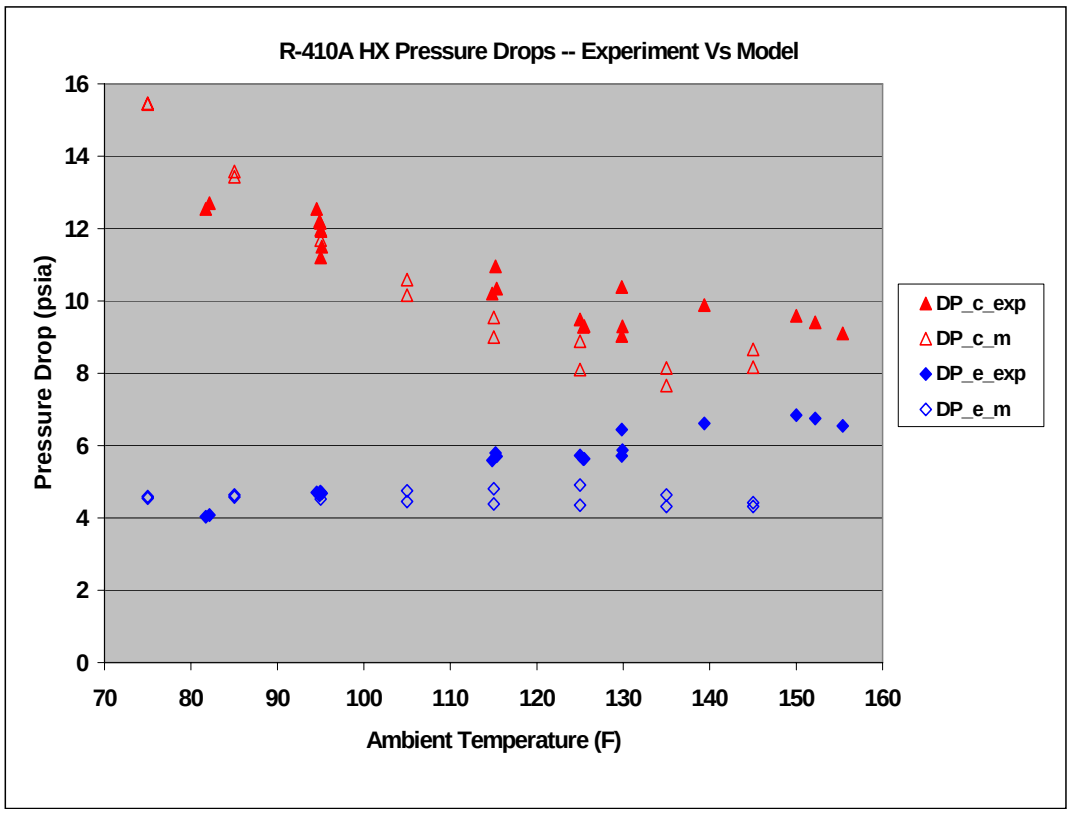

Fig. 37. Measured vs. predicted HX refrigerant pressure drops for R-410A over a wide range of ambient temperature.

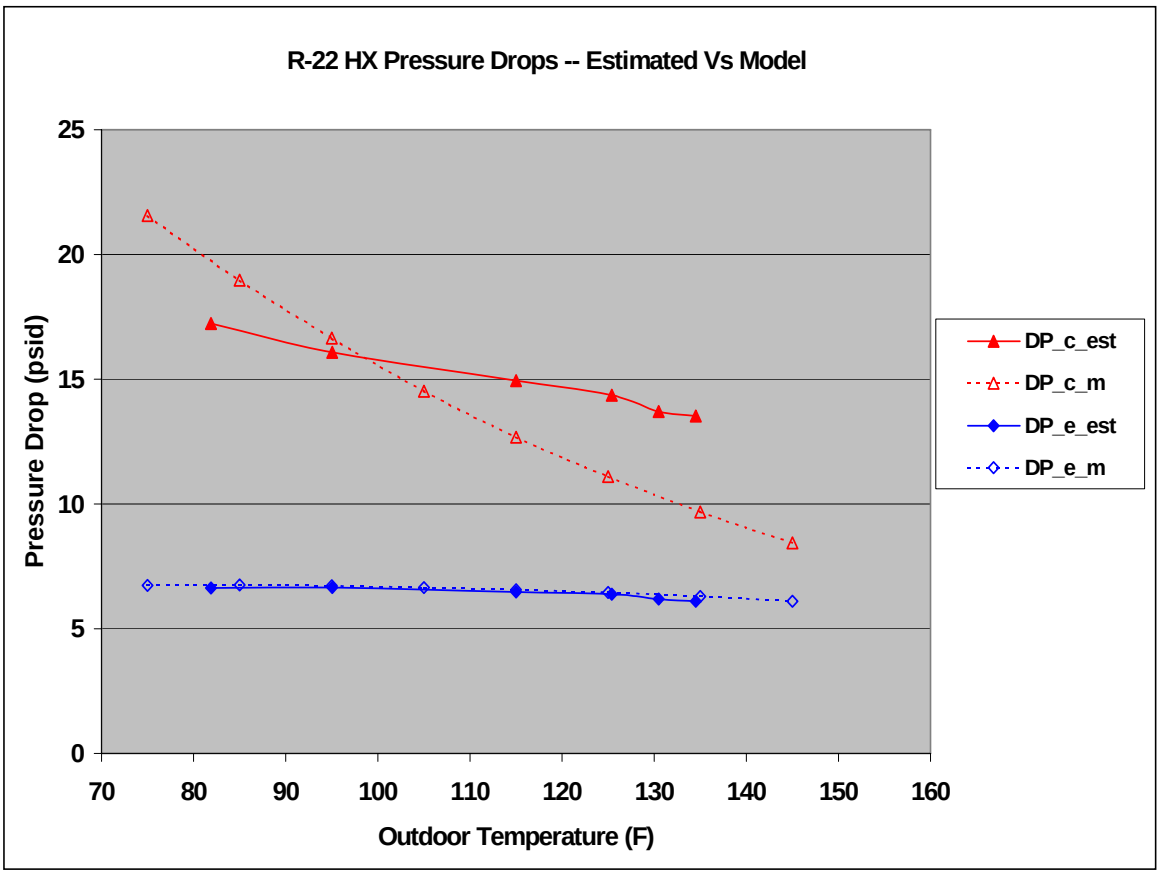

Fig. 38. Estimated vs. predicted HX refrigerant pressure drops for R-22 over a wide range of ambient temperature.

We have had to rely on the model's pressure drop correlations, calibrated to R-410A data at the 95°F calibration point, to predict the increase in pressure drop from the R-410A to the R-22 cases. It is possible that the predicted increases in pressure drop are too high and that this may account to some extent for the poorer agreement with experiment for the R-22 tests than for the R-410A tests. Without accurate HX pressure drop data for the R-22 unit, this cannot be determined.

Next we compare performance ratios of power, capacity, and EER as a function of ambient, normalized to the 95°F design condition for each refrigerant.

These comparisons are shown in Figs. 39–41, where our performance predictions are compared to the performance ratios determined from the measured data. Again, all capacities are based on refrigerant-side and indoor fan power effects are not included. The comparisons are shown for R-22, R-410A with original compressor (Test Series B), and R-410A with modified compressor (Test Series C), respectively. In all three cases, agreement is quite close.

These results show that the final calibrated model predicts the measured relative trends in performance quite closely, based on refrigerant-side capacities and digital power measurements. The absolute differences in performance between model and experiment remain about the same over the test range. (If air-side capacities were used, we would go from under-predicting at the lower to moderate ambient temperatures to over-predicting capacity at the highest temperatures.)

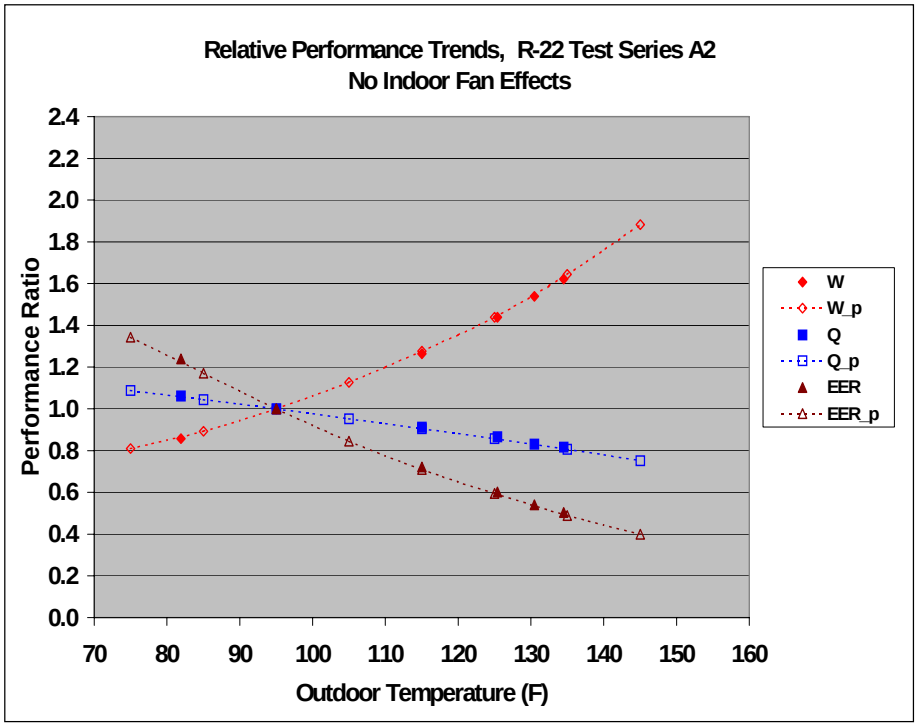

Fig. 39. Measured vs. predicted performance ratios for R-22 over a wide range of ambient temperature.

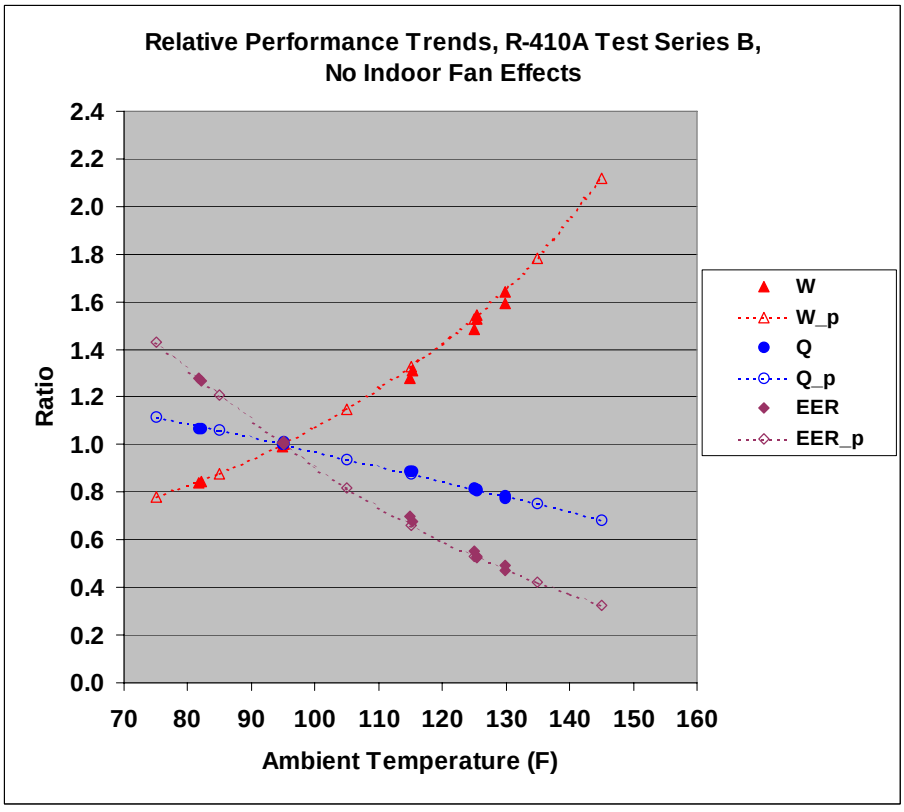

Fig. 40. Measured vs. predicted performance ratios for R-410A, test series B, over a wide range of ambient temperature.

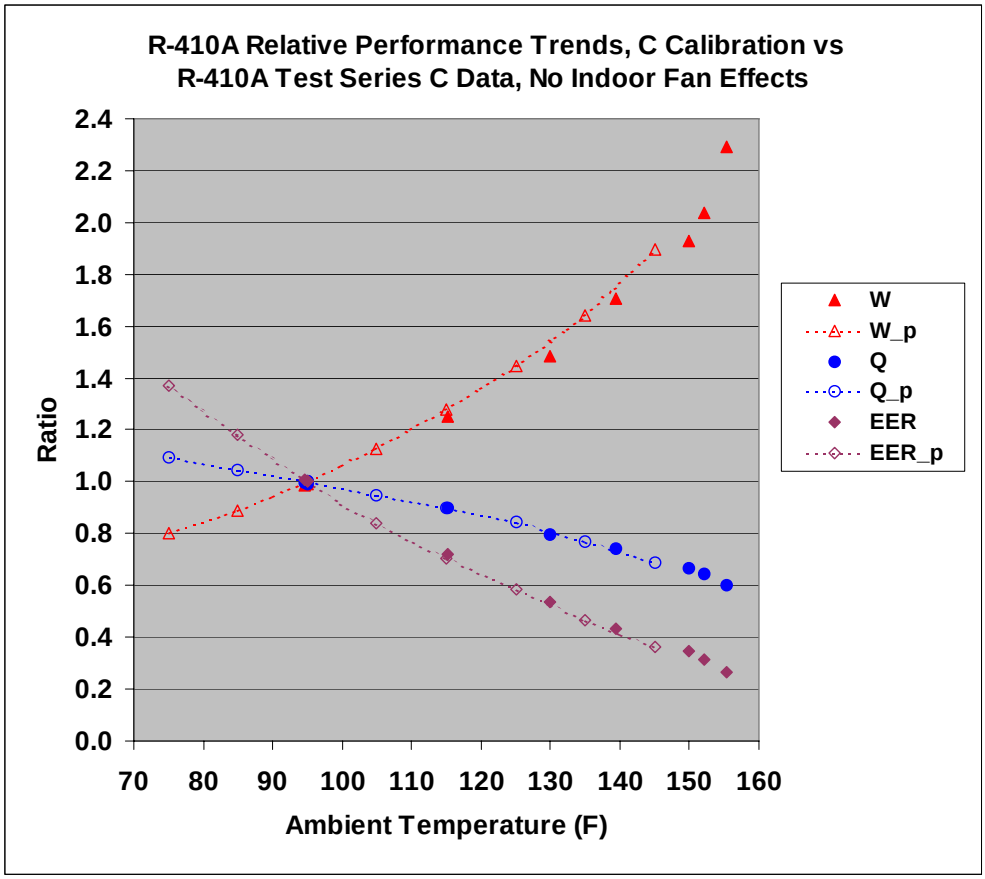

Fig. 41. Measured vs. predicted performance ratios for R-410A, test series C, over a wide range of ambient temperature.

VALIDATED COMPARISONS OF R-410A SYSTEM PERFORMANCE VS. R-22

Next we prepared Figs. 42–44 comparing the predicted performance ratios for R-22 vs. R-410A with the original compressor. In Fig. 42, we show the actual performance ratios as for the earlier plots. In Fig. 43, the percentage change for the R-410A case relative to the R-22 baseline is given. (Note that we have normalized the EER, capacity, and power to the same values for both refrigerants at the 95°F condition for all these plots. Without this normalization, the predicted R-410A values of power, capacity, and EER would have been 1.2, 1.8, and 0.7% higher in Fig. 43.)

These validated trends indicate that at the 145°F ambient, the power for the R-410A condensing unit would be about 12% higher than for a comparable R-22 system (same capacity and EER at 95°F) and that the capacity and EER at 145°F would be about 9% and 19% lower, respectively.

In Fig. 44 we show a comparison of the relative performance results for the initial vs. final calibrated models (Fig. 44 vs. Fig. 16). This shows the degree to which the initial model, calibrated to the design cooling conditions, underestimates the R-410A performance drop-off. This would also represent closely the relative predictions of the manufacturer's extended ratings up to 115°F relative to the measured performance.

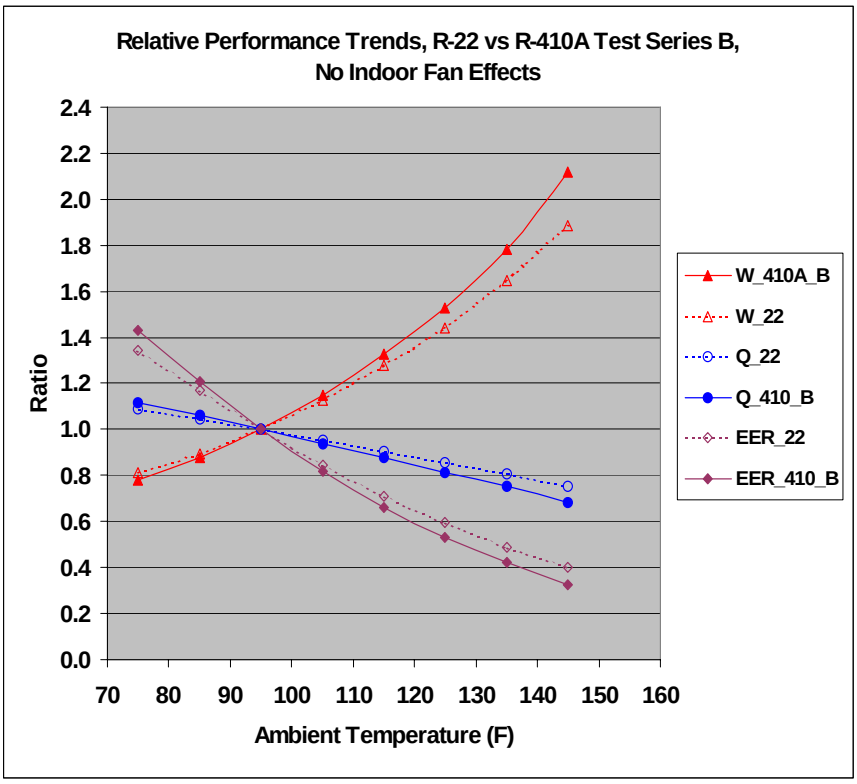

Fig. 42. Predicted performance ratios for R-22 vs. R-410A, test series B, over a wide range of ambient temperature.

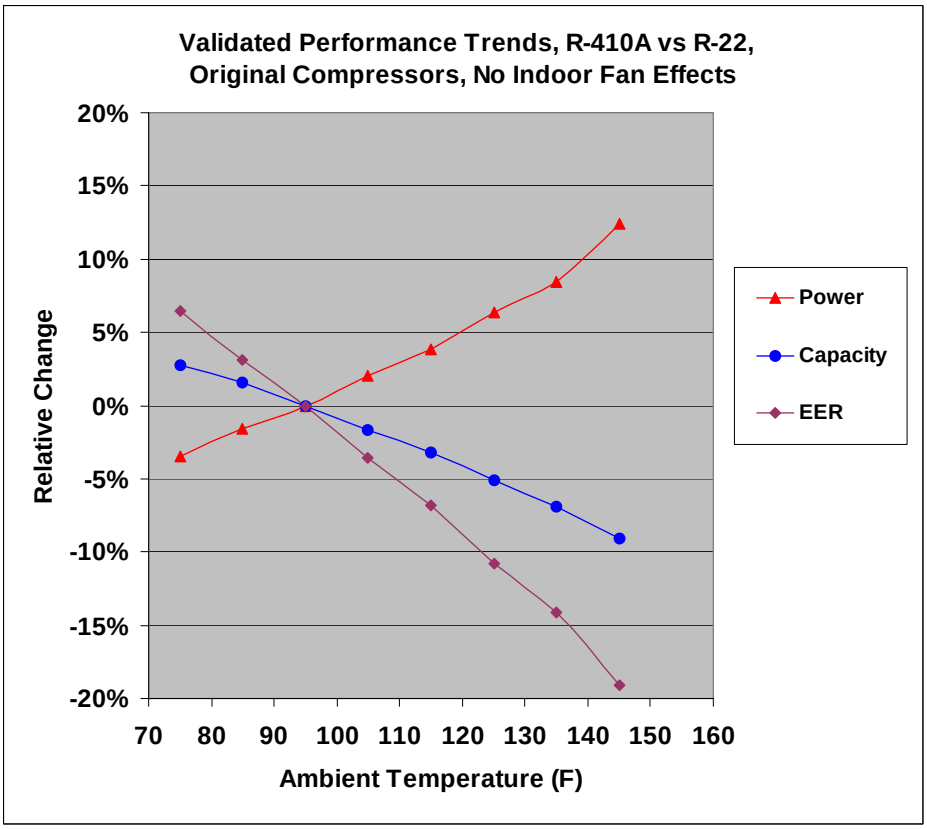

Fig. 43. Validated relative performance differences between R-22 vs. R-410A with original compressors over a wide range of ambient temperature.

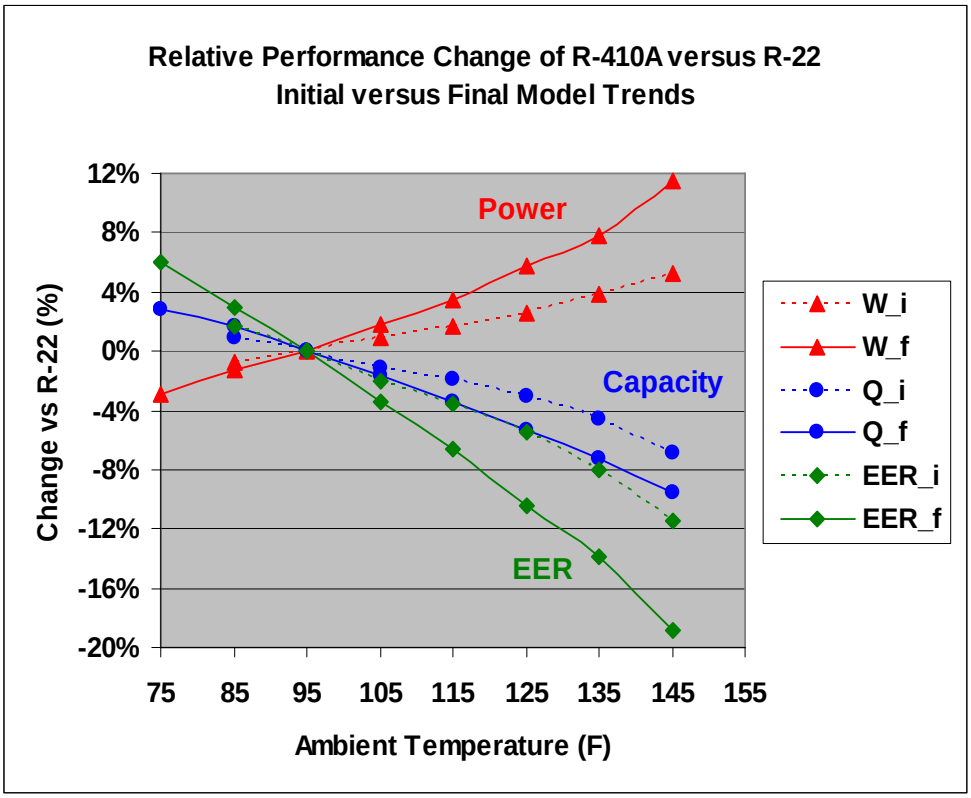

Fig. 44. Initial vs. final calibrated trends for performance drop-off of R-410A vs. R-22 over a wide range of ambient temperature.

SYSTEM PERFORMANCE ANALYSIS WITH DIFFERENT FLOW CONTROLS

Using the calibrated performance models, we next conducted a system performance comparison analysis over the range of conventional flow control devices. For TXVs, we first compared how well our implicit TXV model tracked the measured performance. We then determined the most suitable TXV modeling analysis that would be comparable to fixed-flow control cases for which we had no similar performance data. For the fixed-opening flow control devices, short-tube orifices and capillary tubes, this involved running the calibrated R-22 and R-410A system models at design conditions to size the flow controls. It also involved assessing the need for a suction-line accumulator for these cases. This was followed by conducting full sets of off-design performance predictions with the sized flow controls at fixed design charge levels. This analysis was done for 75 to 145°F ambient temperatures in the cooling mode for fixed- vs. variable-opening (TXV) flow control scenarios. Power, capacity, and EER trends over the full range of ambient temperatures were compared between the different flow controls for R-22 and R-410A.

Implicit TXV Modeling Using Refrigerant Charge Balance

We evaluated measured vs. predicted subcooling trends for TXV flow control using different refrigerant charge balance models. We compared the predicted vs. measured condenser subcooling trends with ambient for the ORNL implicit TXV model using a charge inventory balance with two different HX void fraction models (the ORNL and NIST default methods of

Hughmark and Lockhart-Martinelli, respectively). In the earlier validation analyses, we imposed the measured subcooling (and superheat) trends with ambient rather than trying to predict them.

We found that when using a charge inventory balance with specified superheat to predict TXV performance with R-410A, condenser subcooling is predicted to drop off between 2.5 and more than 3 times the measured loss as the ambient increases (2.6°F measured for R-410A vs. 6.7°F with Hughmark or 8.7°F for L-M). This is shown in Fig. 45, where the Hughmark method tracks the measured trend better at higher ambient temperatures while the L-M approach does better at mild ambient temperatures.

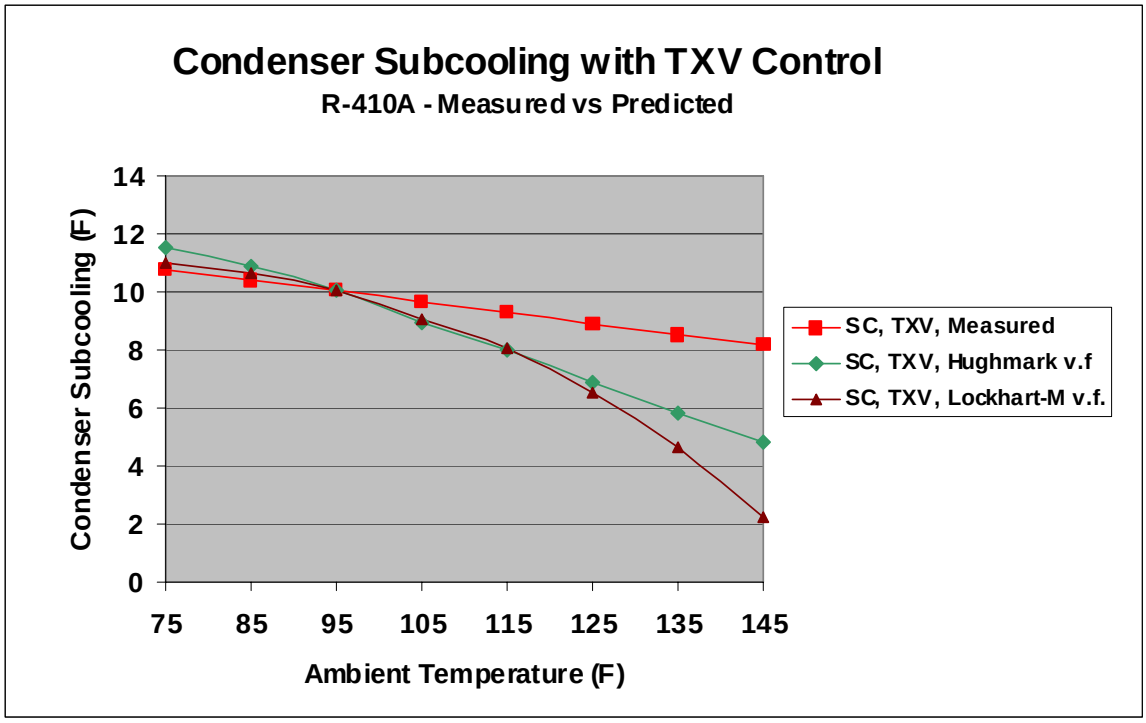

Fig. 45. Comparison of measured vs. predicted subcooling, implicit TXV model with Hughmark or Lockhart-Martinelli void fraction models.

As R-410A performance is more strongly dependent on subcooling than R-22, this will affect to some degree the predicted relative performance at extreme conditions when using implicit TXV models (fixed superheat and refrigerant charge), i.e., when measured subcooling trends are not available to be applied directly in lieu of flow control modeling. This means that the R-410A performance drop-off with ambient would be over-estimated with the charge balance models, relative to R-22.

Even though our charge balance model did not track closely the subcooling trends with ambient temperature for TXV control, we decided to proceed with comparative performance analyses of predicted TXV (variable-opening flow controls) vs. capillary tube and short-tube orifices (fixed-opening flow controls) over the full range of ambient temperatures up to near the critical point for R-410A and R-22. For comparisons between flow controls with the same refrigerant, the predicted relative performance should still be reasonably valid. In all cases, the required refrigerant charge to meet the measured levels of subcooling and superheat at the 95°F rated capacity design point was determined and held fixed for the off-design analysis. For the TXV

case, we assumed also that the compressor inlet superheat trends were held constant (implicit TXV model), while for the fixed-opening flow controls, the required sizes were determined at the design point and specified for the off-design ambient temperatures.

Design Point Sizing and Off-Design Analysis with Fixed-Opening Flow Control Devices

Using the calibrated system models discussed earlier, we sized short-tube orifices and capillary tubes for the tested R-22 and R-410A systems and ran full sets of off-design performance predictions for 75°F to 145°F ambient temperatures for these fixed-opening flow controls. The heat exchanger exit conditions and performance with these flow controls were compared to those with a TXV, in all cases for the same design refrigerant charge.

In Fig. 46, we show the predicted subcooling trends vs. ambient for the fixed-opening flow controls with fixed refrigerant charge as compared to predicted for the implicit TXV model (specified superheat and fixed charge). These results are with suction line accumulators for the capillary tube and short-tube-orifice cases.

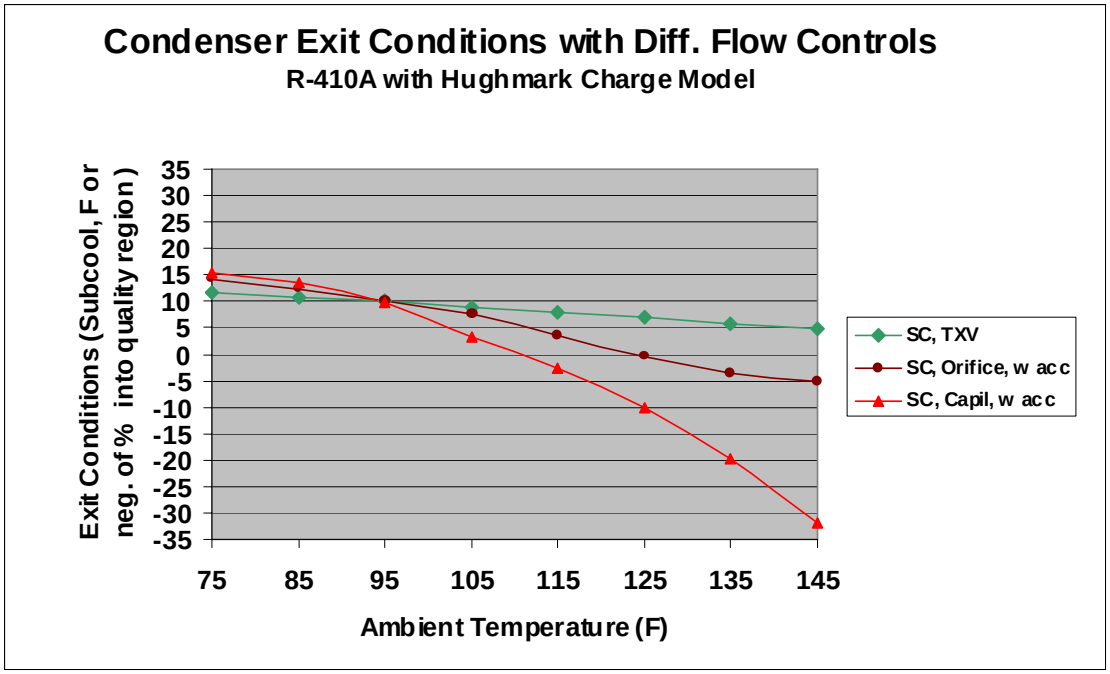

Fig. 46. Comparison of predicted R-410A subcooling-quality trends with ambient for implicit TXV model vs. short-tube orifice and capillary tube flow control with a suction line accumulator.

We analyzed the off-design conditions for fixed-opening flow controls, both with and without suction line accumulators. This is shown in Fig. 47, where evaporator exit superheat or quality, as required, is shown vs. ambient. Without an accumulator, the evaporator exit quality falls to a low of 80% quality with a capillary tube as compared to 92% with a short-tube orifice. Such a low exit quality results in wet compression with significant implications for liquid slugging entering the compressor.

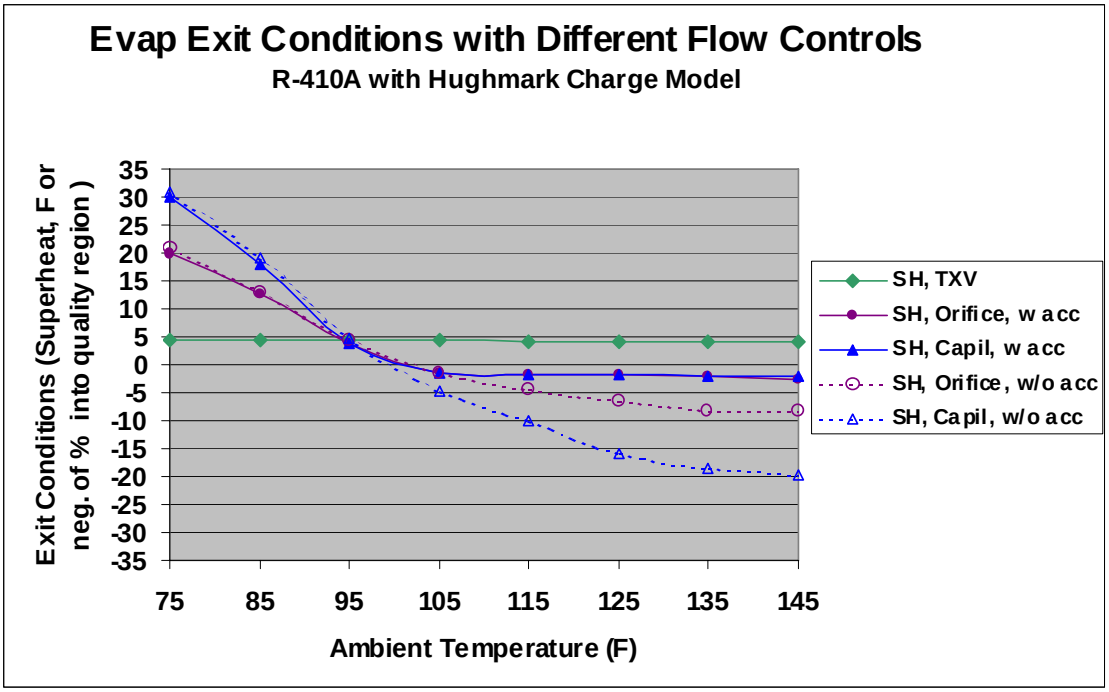

Fig. 47. Comparison of predicted R-410A superheat-quality trends with ambient for implicit TXV model vs. short-tube orifice and capillary tube with and without a suction line accumulator.

With an accumulator, both flow controls maintain an exit quality of about 98% (which should be evaporated by the suction line heat gain and the motor heat before entering the suction port). One result of this is that the condenser subcooling drops faster with ambient than would be the case if an accumulator were not needed. This is shown in Fig. 48, where in the case of no accumulator, more liquid is stored in the condenser to offset the lower exit qualities leaving the evaporator.

The subcooling and superheat trends with ambient were found to be similar for both the R-410A and R-22, but with less drop-off of subcooling with ambient for R-22 than for R-410A. This can be seen by comparing Fig. 48 for R-410A with Fig. 49 for R-22. For the capillary tube case, the condenser exit quality is predicted to drop to 18% for R-22 vs. 32% for R-410A. For short-tube orifices, the condenser exit is predicted to just begin to lose subcooling for R-22 at the highest ambient temperature while operating with up to 13% exit quality for R-410A. Note also that for the capillary tube cases the trend on increasing exit quality is accelerating with ambient, while the loss of subcooling is slowing for the short-tube-orifice control for both refrigerants.

In Fig. 50, the predicted R-22 system performance effects for capillary tubes and short-tube orifices are shown relative to those for a TXV. The EER and capacity for the capillary tube case fall off more than 10% at the mildest and more extreme ambient temperatures compared to a TXV. The power remains about the same at mild temperatures while falling linearly up to 5% at the 145°F ambient.

For the short-tube-orifice case, the drop-off in EER and capacity at higher ambient temperatures is about a third or less of that for the capillary tube, while the power drop-off is about half. At mild ambient temperatures, the drop-off is about 40% of that with capillary tubes.

In Fig. 51, the same comparison is shown for an R-410A system. Here the EER and capacity for the capillary tube case fall off more than 15 to 20%, respectively, at extreme ambient temperatures compared to a TXV. This is larger than for the R-22 system because of (1) the larger

loss of subcooling with ambient, and (2) the larger thermodynamic effect of subcooling loss for R-410A than for R-22. At mild ambient temperatures, R-410A capacity and to some extent EER fall off less than for R-22 because the increased subcooling is more beneficial. For both fixed-opening flow controls, power at higher ambient temperatures falls off faster than with R-22. In contrast, at milder ambient temperatures, the power draw for fixed-opening flow controls is higher than for TXVs with R-410A.

In summary, TXVs maintain EER and especially capacity much better than fixed-flow controls at higher ambient temperatures; however, power draw is increased by 2 to 8% as one potentially negative side effect for utilities. At mild ambient temperatures, near the SEER rating point and below, TXVs. improve EER relative to short-tube orifices and capillary tubes by 4 to 12%, respectively, for R-22, as compared to 3 to 7% for R-410A.

With fixed-opening flow controls, capillary tube performance drops off the most with increasing ambient temperatures with R-410A, next with R-22, followed by short-tube performance with R-410A. For the fixed-flow controls with the needed suction line accumulators, the refrigerant at the condenser exit became or approached two-phase at the higher ambient temperatures, with the capillary tube case losing subcooling at about 110 to 115°F for R-410A and R-22, respectively, while for the short-tube-orifice case subcoooling was maintained until about 125°F ambient for R-410A and up to nearly 145°F for R-22.

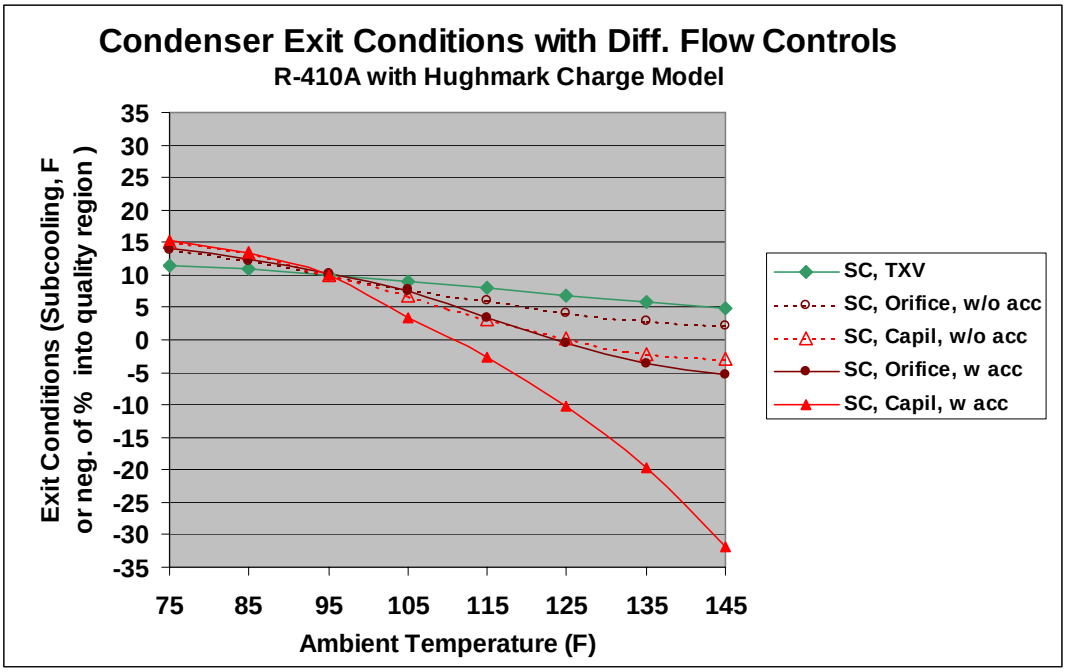

Fig. 48. Comparison of predicted R-410A subcooling-quality trends with ambient for implicit TXV model vs. short-tube orifice and capillary tube flow control with and without a suction line accumulator.

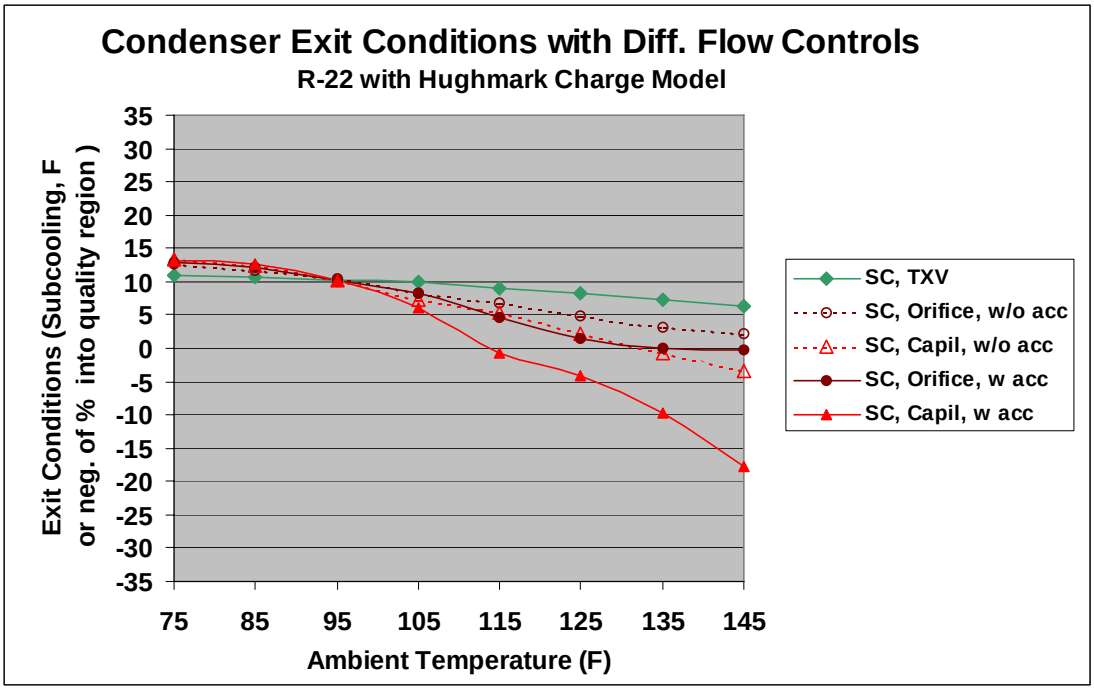

Fig. 49. Comparison of predicted R-22 subcooling-quality trends with ambient for implicit TXV model vs. short-tube orifice and capillary tube flow control with and without a suction line accumulator.

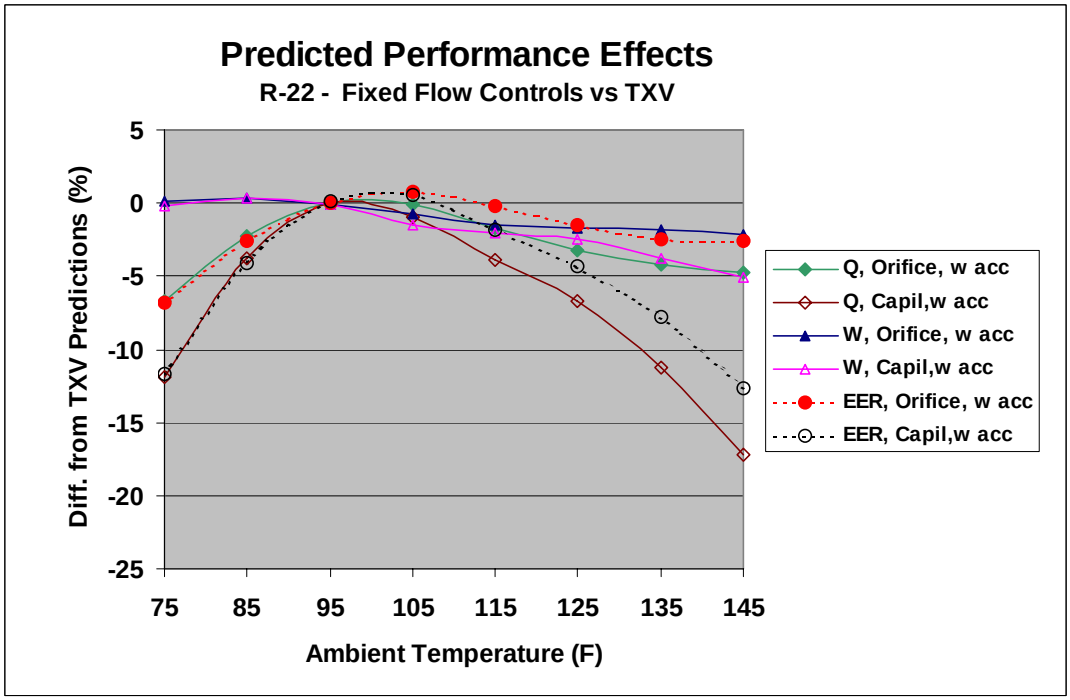

Fig. 50. Comparison of predicted R-22 system performance over a wide range of ambient temperature with fixed-opening flow vs. TXV control.

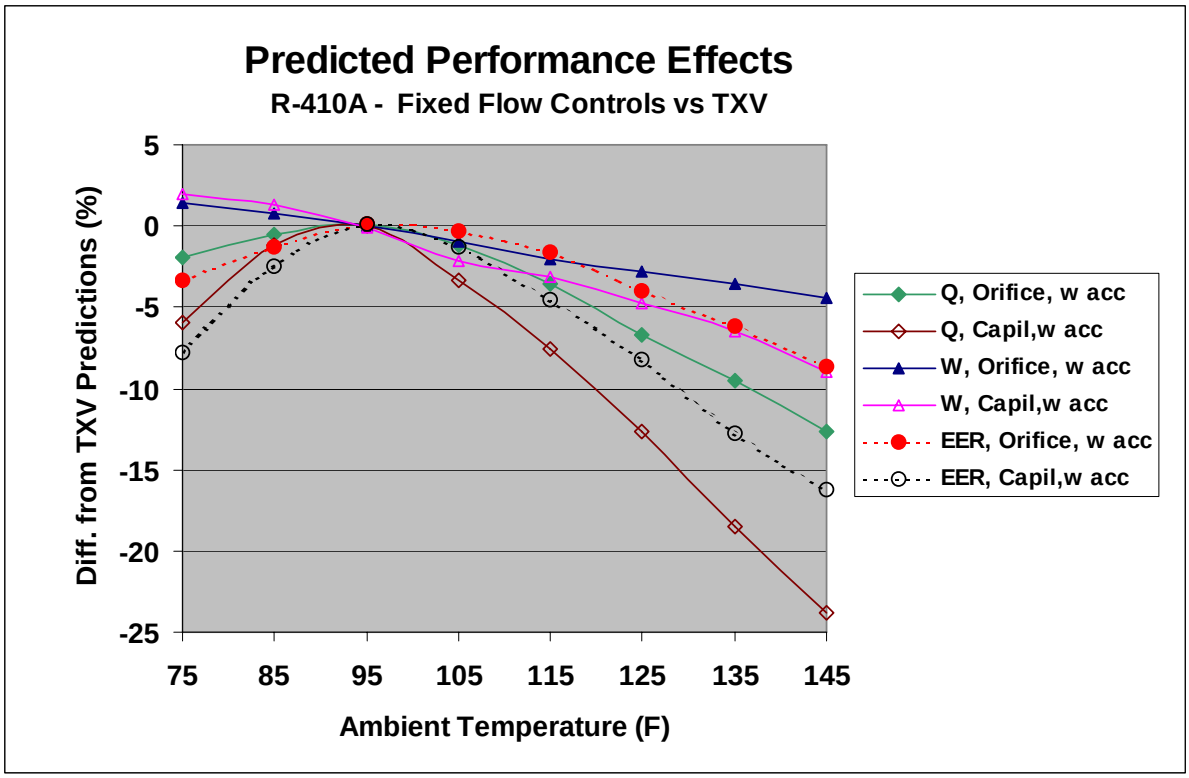

Fig. 51. Comparison of predicted R-410A system performance over a wide range of ambient temperature with fixed-opening flow vs. TXV control.

SUMMARY OF PROJECT ACCOMPLISHMENTS

- Made a number of model improvements related to more accurate modeling at elevated ambient temperatures with R-410A.
- Developed wide-range R-410A scroll compressor maps that could be used up to and beyond the critical temperature.
- Analyzed relative performance of R-22 and R-410A compressors and systems tested in-situ using NIST data.
- Using NIST system test data, characterized the performance of the in-situ system-tested compressors relative to the manufacturer's maps, accounting separately for effects of reduced voltage and reduced airflow over the shell, with regard to power, mass flow, and shell heat loss corrections.
- Developed calibrated models for comparing R-410A to R-22 performance in the same equipment hardware for ambient temperatures up to and exceeding 135°F. Compared this to a model calibrated to a single ambient temperature and to manufacturer's extended ratings data.

- Added to our system model the capability to specify compressor map power and mass flow adjustment factors, compressor shell heat loss, suction, discharge, and liquid line pressure drops as a function of ambient temperature. These capabilities were implemented in the Web version of the Mark VI HPDM and made available on line at www.ornl.gov/~wlj/hpdm/MarkVI.shtml as ambient control options. This was a key deliverable for this project. Model improvements are also documented on line in the Web model at www.ornl.gov/~wlj/hpdm/Mark_VI_Notes.html.

- Determined the relative performance of R-410A vs. R-22 with TXV control with respect to power, capacity, and EER from 75 to 145°F ambient temperature. Compared relative performance drop-offs with TXV control to that with capillary tubes and short-tube orifices.

SUMMARY FINDINGS

We demonstrated that the Mark VI DOE/ORNL HPDM could successfully model the performance of R-410A systems at ambient temperatures up to 145°F and for condensing temperatures within 0.5 degrees of critical. However, we found that compressor performance calibration factors that increased with ambient temperature were required for a good match of performance trends and that liquid line heat losses needed to be accounted for properly.

It was found that compressor performance changes relative to the map predictions can be significant at elevated ambient temperatures and that operating voltage corrections especially need to be applied at these conditions. As the compressor maps are developed for 95°F air blowing over a compressor, elevated ambient temperatures and, even more significantly, reduced airflow over the compressor are expected to be the main reasons for these differences. We compared the compressor shell heat loss in system tests to those from manufacturer's calorimeter tests and found approximately a 50% reduction. This finding helps to explain the lower compressor performances relative to the maps. A consistent loss in mass flow rate was seen vs. the compressor maps at higher ambient temperatures along with a trend of increasing power draw relative to the predicted map performance. The net effect is a significant drop-off in compressor EER relative to the maps. This suggests that the motor is running less efficiently from running hotter and that the suction gas is also picking up more heat, reducing suction density and thus capacity. These observations indicated the need for correction factors to be applied to map power and mass flow values as a function of ambient temperature. Shell heat loss fractions (fractions of input power) also varied with ambient temperature, and this was tracked in the corrected model to better match the required condenser heat rejection loads at elevated ambient temperatures.

We found that liquid line heat losses could be considerable at higher ambient temperatures and need to be suitably accounted for in simulations. The effect of line heat losses is to increase the level of subcooling with ambient temperature seen by the flow control as compared to that leaving the condenser, which has an opposite, slightly decreasing trend with ambient temperature.

It appeared that there was excessive pressure drop in the liquid line of the R-410A test cases, possibly in the filter/dryer. This may have caused the condenser pressures to be more elevated than they should have been.

We found that TXV flow control modeled using measured superheat levels and fixed refrigerant charge over-predicts the drop-off in condenser subcooling as ambient temperature increase. The recommended way to model TXV systems at present, in lieu of experimental data, is to simply fix the subcooling and superheat at design levels for all ambient temperatures, or to assume that they change only by a few degrees with ambient based on the findings of lab tests for one representative unit such as available to this project.

We found that while TXV systems maintain capacity and EER better than fixed-opening flow controls, this does result in a higher compressor power draw. At ambient temperatures where the unit will be running 100% of the time, this will result in higher peak power requirements than the fixed-opening flow control systems which tend to slow power draw increases but provide less capacity at extreme ambient temperatures.

We found that the recommended *ASHRAE Handbook* method for modeling capillary tube performance with R-410A is flawed and will mis-predict refrigerant flow by 10% or more. We also found that more test data at higher pressures and subcooling levels are needed to extend these models for use at high ambient cooling conditions with R-410A.

We found that the uncorrected model over-predicts relative R-410A performance at higher ambient temperatures.

The loss in R-410A performance is greater primarily due to larger drops in compressor performance than predicted. At 125°F ambient, relative to R-22, we found an 11% larger drop in EER and 5% drop in capacity, with a 6% larger increase in power.

The model is capable of use up to the critical point. It can give good agreement with test data when suitable derating factors are provided for reduced compressor performance at elevated ambient temperatures.

TXV control has less drop-off in EER and capacity at higher ambient temperatures than with fixed-flow controls, especially compared to capillary tube control. This is primarily due to the smaller drop in subcooling with ambient temperature. However, power draw for TXV is higher than for fixed-flow controls since higher condenser pressures are maintained at elevated ambient temperatures.

RECOMMENDATIONS

There is a need for further data to develop correlations on how compressor performance is affected by air-over temperature and airflow. Shell loss seems to be more affected by airflow over the shell than ambient air temperature. This would provide a much better basis for extrapolating system performance to higher ambient temperatures.

We recommend that compressor tests be done at elevated ambient temperatures with airflow over compressor and in enclosures typical of outdoor unit application to quantify these effects on compressor power and mass flow rate. Models of these effects need to be developed and incorporated into simulation models used to predict the performance of unitary equipment at elevated ambient temperatures seen at peak utility conditions.

We recommend research to develop suitable derating correlations for compressors operating at elevated ambient temperatures. These should be based on airflow and ambient conditions seen by the compressor as compared to standard airflow over compressor at 95°F ambient. The data studied here suggest that the losses from these effects are larger for R-410A than for R-22. Presently in-situ test data are needed to determine suitable corrections. Clearly, there is a need for better models to predict these effects on peak power draws and performance at elevated ambient temperatures. This should be considered as a possible ARTI or ASHRAE research project.

The measured line losses from the NIST tests should be compared to existing ASHRAE and ASTM line loss models. A calibrated model for line losses should be added to the DOE/ORNL HPDM. Improved refrigerant line heat loss modeling will provide better prediction of absolute performance at more extreme ambient temperatures.

It is recommended that improvements be made to capillary tube modeling for R-410A for higher pressures and larger diameter capillary tubes. Equally important, the ASHRAE generalized correlation for capillary tubes in the current handbook needs to be corrected for errors in the viscosity effects due to the use of incorrect properties when the correlations were developed.

We recommend adding new flow control models for variable-opening short-tube orifices, which increase restriction at higher condenser pressures, and evaluating how well these devices can approach the performance of TXV systems. Such devices have the potential to maintain subcooling better than fixed orifices and thus maintain higher performance at elevated ambient temperature, while still being a lower cost alternative to TXVs.

Further improvements are needed in charge inventory modeling and/or modeling of the condenser subcooled HX length changes with ambient temperature to more accurately model, on an absolute basis, the changes in charge requirement and thereby in predicted HX exit subcooling and superheat levels with ambient temperature with fixed-opening and especially variable-opening devices such as TXVs.

REFERENCES

Air-Conditioning and Refrigeration Institute, 1999. *Positive Displacement Compressors and Compressor Units*, ANSI/ARI Standard 540-1999, p.2-3.

Allied-Signal, 1993. Personal communication, M. Spatz.

For Allied-Signal transport properties for refrigerant mixtures, the following references were used in conjunction with internally generated component properties:

L. P. Filippov, 1955. Vest. Mosk. Univ., *Ser. Fiz. Mat. Estestv. Nauk.*, Vol. 8, pp. 67-69, (Liquid thermal conductivity of mixtures).

Jung, D. S., and D. A. Didion, 1990. "A Mixing Rule For Liquid Viscosities of Refrigerant Mixtures," *International Journal of Refrigeration*, Vol. 13, pp. 243-247 (liquid viscosity of mixtures).

Nagaoka, K., Y. Tanaka, H. Kubota, and T. Makita, 1986. "A New Correlation for Viscosity of Gaseous Fluorocarbon Refrigerants," *International Journal of Thermophysics*, Vol. 7, No. 5, pp. 1023-1031 (Vapor viscosity of pure and mixed refrigerants).

ASHRAE, 1976. *Thermophysical Properties of Refrigerants, Second Edition.*

ASHRAE, 1993. *Thermophysical Properties of Refrigerants, (Inch-Pound Edition).*

ASHRAE, 1998. *1998 ASHRAE Handbook, Refrigeration*, *IP-Edition*, pp. 45.24-45.27.

Assael, M. J., et al, 1999. "Viscosity and Thermal Conductivity of Halogenated Methane and Ethane Refrigerants," *International Journal of Refrigeration*, Vol. 22, pp. 525-535.

Bittle, R. R., D. A. Wolf, and M. B. Pate, 1998. "A Generalized Performance Prediction Method for Adiabatic Capillary Tubes," *HVAC&R Research* , Vol. 4, No. 1, January, pp. 27-44.

Bivens, D. B., and A. Yokozeki, 1994. "Heat Transfer Coefficients and Transport Properties for Alternative Refrigerants," International Refrigeration Conference Proceedings, Purdue University.

Dobson, M. K., et al., May 1994. *Heat Transfer and Flow Regimes During Condensation in Horizontal Tubes*, ACRC TR-57, Univ. of Illinois.

Domanski, P. A., and W. V. Payne, October 2002. *Properties and Cycle Performance of Refrigerant Blends Operating Near and Above the Refrigerant Critical Point, Task 2: Air Conditioner System Study.* NIST, ARTI-21CR/605-50010-01-Pt. 2.

DuPont, 1999. "Accurate Engineering Equations for Thermodynamic Properties: Part II. "R-410A," Personal communication with C. K. Rice, A. K. Yokozeki.

DuPont, 1995. *Transport Properties of SUVA 9100 Refrigerant,* SUVA Refrigerants Product Information, ART-31, September. *Note: Initially developed for R410B (55% R-125, 45% R-32). Quoted upper limit of correlations is 150°F.*

Geller, V. Z., B. V. Nemzer, and U. V. Cheremnykh, 2000. "Thermal Conductivity of Mixed Refrigerants," *14th Symposium on Thermophysical Properties*, June 25-30, 2000, Boulder, Colorado.

Geller, V. Z., D. Bivens, and A. Yokozeki, 2000. "Viscosity of Mixed Refrigerants R404A, R407C, R410A, and R507A," *8th International Refrigeration Conference at Purdue University*, West Lafayette, Indiana, USA, July 25-28, 2000, pp. 399-406.

Geller, V, 2002. Transport Properties for Refrigerant Blends, ASHRAE Research Project TRP-1142.

Goldstein, S. D., 1979. "On the Calculation of R-22 Pressure Drop in HVAC Evaporators," *ASHRAE Transactions*, Vol. 85, Part 2.

Klein, S. A., and F. L. Alvarado, 1999. *EES, Engineering Equation Solver for the Microsoft Operating System*, F-Chart Software.

Klein, S. A., and F. L. Alvarado, 2000. *EES, Engineering Equation Solver for the Microsoft Operating System*, F-Chart Software.

McLinden, M. O., S. A. Klein, E. A. Lemmon, and A. P. Peskin, 1999. *NIST Thermodynamic and Transport Properties of Refrigerants and Refrigerant Mixtures—RefProp, Version 6.01*. (Note: Current upper limit on saturated calculations for R-410A is 152.5°F).

NIST, 2001. Personal communication with W. Vance Payne to C.K. Rice, Jan-Nov.

Payne, W. Vance, and D. L. O'Neal, June 1999. "Multiphase Flow of Refrigerant 410A Through Short-Tube Orifices," *ASHRAE Transactions*, Vol. 105, Part 2.

Payne, W. Vance, 1997. *A Universal Mass Flowrate Correlation for Refrigerants and Refrigerant/Oil Mixtures Flowing Through Short-Tube Orifices*, Ph. D. Dissertation, Texas A&M, May.

Rice, C. K., and W. L. Jackson, 1994. *PUREZ — The Mark V ORNL Heat Pump Design Model For Chlorine-Free, Pure and Near-Azeotropic Refrigerant Alternatives, Documentation Package, Version 0.95B*, Oak Ridge National Laboratory, November.

Wattelet, J. P., et al., June 1993. *Initial Evaporative Comparison of R-22 with Alternative Refrigerants R134a and T-32/R-125*, ACRC TR-39, Univ. of Illinois.

Wolf, D. A., R. R. Bittle, and M. B. Pate, 1995. *Adiabatic Capillary Tube Performance with Alternative Refrigerants, ASHRAE RP-762, Final Report*, Engineering Research Institute, Iowa State University, ERI-95413, May.